

**Reviews and syntheses:**  
**The biogeochemical cycle of silicon in the modern ocean**

Paul J. Tréguer<sup>1,2\*</sup>, Jill N. Sutton<sup>1</sup>, Mark Brzezinski<sup>3</sup>, Matthew A. Charette<sup>4</sup>, Timothy Devries<sup>5</sup>, Stephanie Dutkiewicz<sup>6</sup>, Claudia Ehlert<sup>7</sup>, Jon Hawkings<sup>8,9</sup>, Aude Leynaert<sup>1</sup>, Su Mei Liu<sup>10,11</sup>, Natalia Llopis Monferrer<sup>1</sup>, María López-Acosta<sup>12,13</sup>, Manuel Maldonado<sup>13</sup>, Shaily Rahman<sup>14</sup>, Lihua Ran<sup>15</sup>, Olivier Rouxel<sup>16</sup>

<sup>1</sup>Univ Brest, CNRS, IRD, Ifremer, Institut Universitaire Européen de la Mer, LEMAR, Rue Dumont d'Urville, 29280, Plouzané, France

<sup>2</sup>State Key Laboratory of Satellite Ocean Dynamics (SOED), Ministry of Natural Resource, Hangzhou 310012, China

<sup>3</sup>Marine Science Institute, University of California, Santa Barbara, CA, USA

<sup>4</sup>Department of Marine Chemistry and Geochemistry, Woods Hole Oceanographic Institution, Woods Hole, MA 02543 USA

<sup>5</sup>Department of Geography, University of California, Santa Barbara, California, USA

<sup>6</sup>Department of Earth, Atmospheric and Planetary Sciences (DEAPS), Massachusetts Institute of Technology (MIT), Cambridge, MA 02139, USA

<sup>7</sup>Research Group for Marine Isotope Geochemistry, Institute for Chemistry and Biology of the Marine Environment (ICBM), Carl-von Ossietzky University Oldenburg, Germany

<sup>8</sup>National High Magnetic Field Lab and Earth, Ocean and Atmospheric Sciences, Florida State University, USA

<sup>9</sup>Interface Geochemistry, German Research Centre for Geosciences GFZ, Potsdam, Germany

<sup>10</sup>Frontiers Science Center for Deep Ocean Multispheres and Earth System, and Laboratory of Marine Chemistry Theory and Technology MOEY, Ocean University of China, Qingdao 266100, China

<sup>11</sup>Laboratory for Marine Ecology and Environmental Science, Qingdao National Laboratory for Marine Science and Technology, Qingdao 266237, China

29 <sup>12</sup>Institute of Marine Research (IIM-CSIC), Rúa de Eduardo Cabello 6, Vigo 36208,  
30 Pontevedra, Spain

31 <sup>13</sup>Department of Marine Ecology. Center for Advanced Studies of Blanes (CEAB-CSIC),  
32 Acceso Cala St. Francesc 14, Blanes 17300, Girona, Spain

33 <sup>14</sup>Department of Marine Science, University of Southern Mississippi, Stennis Space Center, MS  
34 39529, USA

35 <sup>15</sup>Second Institute of Oceanography, Ministry of Natural Resources, P. R. China

36 <sup>16</sup>IFREMER, Centre de Brest, Technopôle Brest Iroise, Plouzané, France

37 Correspondance: Paul Tréguer ([paul.treguer@univ-brest.fr](mailto:paul.treguer@univ-brest.fr)) and Jill Sutton ([jill.sutton@univ-](mailto:jill.sutton@univ-brest.fr)  
38 [brest.fr](mailto:jill.sutton@univ-brest.fr))  
39

## Abstract

The element silicon (Si) is required for the growth of silicified organisms in marine environments, such as diatoms. These organisms consume vast amounts of Si together with N, P, and C, connecting the biogeochemical cycles of these elements. Thus, understanding the Si cycle in the ocean is critical for understanding wider issues such as carbon sequestration by the ocean's biological pump. In this review, we show that recent advances in process studies indicate that total Si inputs and outputs, to and from the world ocean, are 57 % and 37 % higher, respectively, than previous estimates. We also update the total ocean silicic acid inventory value, which is about 24% higher than previously estimated. These changes are significant, modifying factors such as the geochemical residence time of Si, which is now about 8,000 years, two times faster than previously assumed. In addition, we present an updated value of the global annual pelagic biogenic silica production ( $255 \text{ Tmol-Si yr}^{-1}$ ) based on new data from 49 field studies and 18 model outputs, and provide a first estimate of the global annual benthic biogenic silica production due to sponges ( $6 \text{ Tmol-Si yr}^{-1}$ ). Given these important modifications, we hypothesize that the modern ocean Si cycle is at approximately steady state with inputs =  $14.8 (\pm 2.6) \text{ Tmol-Si yr}^{-1}$  and outputs =  $15.6 (\pm 2.4) \text{ Tmol-Si yr}^{-1}$ . Potential impacts of global change on the marine Si cycle are discussed.

## 1. Introduction

Silicon, the seventh-most abundant element in the universe, is the second most abundant element in the Earth's crust. The weathering of the Earth's crust by  $\text{CO}_2$ -rich rain water, a key process in the control of atmospheric  $\text{CO}_2$  (Berner et al., 1983; Wollast & Mackenzie, 1989), results in the generation of silicic acid ( $\text{dSi}$ ;  $\text{Si}(\text{OH})_4$ ) in aqueous environments. Silicifiers are among the most important aquatic organisms, and include micro-organisms (e.g. diatoms, rhizarians, silicoflagellates, several species of choanoflagellates), and macro-organisms (e.g. siliceous sponges). Silicifiers use  $\text{dSi}$  to precipitate biogenic silica ( $\text{bSi}$ ;  $\text{SiO}_2$ ) as internal (Moriceau et al., 2019) and/or external (Maldonado et al., 2019) structures. Phototrophic silicifiers, such as diatoms, globally consume vast amounts of Si concomitantly with nitrogen (N), phosphorus (P) and inorganic carbon (C), connecting the biogeochemistry of these elements and contributing to the sequestration of atmospheric  $\text{CO}_2$  in the ocean (Tréguer & Pondaven, 2000). Heterotrophic organisms like rhizarians, choanoflagellates and sponges produce  $\text{bSi}$  independently of the photoautotrophic processing of C and N (Maldonado et al., 2012, 2019; Llopis Monferrer et al., 2020).

Supprimé: e

Mis en forme : Exposant

Supprimé: e

Mis en forme : Exposant

Supprimé: o

Supprimé: , and  $\text{bSi}$

Understanding the Si cycle is critical for understanding the functioning of marine food webs, biogeochemical cycles, and the biological carbon pump. Herein, we review recent advances in field observations and modelling that have changed our understanding of the global Si cycle and provide an update of four of the six net annual input fluxes and of all the output fluxes previously estimated by Tréguer & De La Rocha (2013). Taking into account numerous field studies in different marine provinces and model outputs, we re-estimate the Si production (Nelson et al., 1995), review the potential contribution of rhizarians (Llopis Monferrer et al., 2020) and picocyanobacteria (Ohnemus et al., 2016), and give an estimate of the total bSi production by siliceous sponges using recently published data on sponge bSi in marine sediments (Maldonado et al., 2019). We discuss the question of the balance/imbalance of the marine Si biogeochemical cycle at different time scales, and we hypothesize that the modern ocean Si cycle is potentially at steady state with inputs =  $14.8 (\pm 2.6) \text{ Tmol-Si yr}^{-1}$  approximately balancing outputs =  $15.6 (\pm 2.4) \text{ Tmol-Si yr}^{-1}$  (Fig. 1). Finally, we address the question of the potential impact of anthropogenic activities on the global Si cycle and suggest guidelines for future research endeavours.

## 2. Advances in input fluxes

Silicic acid is delivered to the ocean through six pathways as illustrated in Fig. 1, which all ultimately derive from the weathering of the Earth's crust (Tréguer & De La Rocha, 2013). All fluxes are given with an error of one standard deviation.

### 2.1 Riverine ( $F_R$ ) and Aeolian ( $F_A$ ) contributions

The best estimate for the riverine input ( $F_R$ ) of dSi, based on data representing 60% of the world river discharge and a discharge-weighted average dSi riverine concentration of  $158 \mu\text{M-Si}$  (Dürr et al., 2011), remains at  $F_{RdSi} = 6.2 (\pm 1.8) \text{ Tmol-Si yr}^{-1}$  (Tréguer & De La Rocha, 2013). However, not only dSi is transferred from the terrestrial to the riverine system, with particulate Si mobilised in crystallised or amorphous forms (Dürr et al., 2011). According to Saccone et al. (2007), the term “amorphous silica” (aSi) includes biogenic silica (bSi, from phytoliths, freshwater diatoms, sponge spicules), altered bSi, and pedogenic silicates, the three of which can have similar high solubilities and reactivities. Delivery of aSi to the fluvial system has been reviewed by Frings et al. (2016) and they suggested a value of  $F_{RaSi} = 1.9 (\pm 1.0) \text{ Tmol-Si yr}^{-1}$ . Therefore, total  $F_R = 8.1 (\pm 2.0) \text{ Tmol-Si yr}^{-1}$ .

No progress has been made regarding aeolian dust deposition into the ocean (Tegen & Kohfeld, 2006) and subsequent release of dSi via dust dissolution in seawater since Tréguer and De La Rocha (2013), which summed the flux of particulate dissolvable silica and wet deposition of

Supprimé: e

Supprimé: e

dSi through precipitations. Thus, our best estimate for the aeolian flux of dSi,  $F_A$ , remains 0.5 ( $\pm 0.5$ ) Tmol-Si yr<sup>-1</sup>.

## 2.2 Dissolution of minerals ( $F_w$ )

As shown in Fig. 2, the low-temperature dissolution of siliceous minerals in seawater and from sediments feeds a dSi flux,  $F_w$ , through two processes: (1) the dissolution of river-derived lithogenic particles deposited along the continental margins and shelves, and (2) the dissolution of basaltic glass in seawater, processes that work mostly in deep waters. About 15-20 Gt yr<sup>-1</sup> of river-derived lithogenic particles are deposited along the margins and shelves (e.g. Syvitskia et al., 2003, also see Fig. 2). Dissolution experiments with river sediments or basaltic glass in seawater showed that 0.08-0.17% of the Si in the solid phase was released within a few days to months (e.g., Jones et al., 2012; Morin et al., 2015; Oelkers et al., 2011; Pearce et al., 2013). However, the high solid-to-solution ratios in these experiments increased the dSi concentration quickly to near-equilibrium conditions inhibiting further dissolution, which prevents direct comparison with natural sediments. Field observations and subsequent modelling of Si release range around 0.5 – 5% yr<sup>-1</sup> of the Si originally present in the solid phase dissolved into the seawater (e.g., Arsouze et al., 2009; Jeandel and Oelkers, 2015). On the global scale, Jeandel et al. (2011) estimated the total flux of dissolution of minerals to range between 0.7 - 5.4 Tmol-Si yr<sup>-1</sup>, i.e. similar to the dSi river flux. However, this estimate is based on the assumption of 1-3% congruent dissolution of sediments for a large range of lithological composition which, so far, has not been proven.

Another approach to estimate  $F_w$  is to consider the benthic efflux from sediments devoid of biogenic silica deposits. Frings (2017) estimates that “non-biogenic silica” sediments (i.e. clays and calcareous sediments, which cover about 78% of the ocean area) may contribute up to 44.9 Tmol-Si yr<sup>-1</sup> via a benthic diffusive Si flux. However, according to lithological descriptions given in GSA Data Repository 2015271 some of the “non-biogenic silica” sediment classes described in this study may contain significant bSi, which might explain this high estimate for  $F_w$ . Tréguer and De La Rocha (2013) considered benthic efflux from non-siliceous sediments ranging between ~10-20 mmol m<sup>-2</sup> yr<sup>-1</sup>, in agreement with Tréguer et al. (1995). If extrapolated to 120 M km<sup>2</sup> zone of opal-poor sediments in the global ocean, this gives an estimate of  $F_w$  = 1.9 ( $\pm 0.7$ ) Tmol-Si yr<sup>-1</sup>.

## 2.3 Submarine groundwater ( $F_{gw}$ )

Since 2013, several papers have sought to quantify the global oceanic input of dissolved Si (dSi) from submarine groundwater discharge (SGD), which includes terrestrial (freshwater) and marine (saltwater) components (Fig. 2). Silicic acid inputs through SGD may be considerable,

similar to or in excess of riverine input in some places. For instance, Georg et al. (2009) estimated this input to be  $0.093 \text{ Tmol-Si yr}^{-1}$  in the Bay of Bengal, which is  $\sim 66\%$  of the Ganges-Brahmaputra river flux of dSi to the ocean. At a global scale Tréguer and De La Rocha (2013)'s best estimate for  $F_{\text{GW}}$  was  $0.6 (\pm 0.6) \text{ Tmol-Si yr}^{-1}$ . More recently, Rahman et al. (2019) used a global terrestrial SGD flux model weighted according to aquifer lithology (Beck et al., 2013) in combination with a compilation of dSi in shallow water coastal aquifers to derive a terrestrial groundwater input of dSi to the world ocean of  $0.7 (\pm 0.1) \text{ Tmol-Si yr}^{-1}$ . This new estimate, with its relatively low uncertainty, represents the lower limit flux of dSi to the ocean via SGD. The marine component of SGD, driven by a range of physical processes such as density gradients or waves and tides, is fed by seawater that circulates through coastal aquifers or beaches via advective flow paths (Fig. 2; also see Fig. 1 of Li et al., 1999). This circulating seawater may become enriched in dSi through bSi or mineral dissolution, the degree of enrichment being determined by subsurface residence time and mineral type (Anschutz et al., 2009; Ehlert et al. 2016a; Techer et al., 2001).

Several lines of evidence show that the mineral dissolution (strictly corresponding to net dSi input) may be substantial (e.g., Ehlert et al., 2016b). Focusing on processes occurring in tidal sands, Anschultz et al. (2009) showed that they can be a biogeochemical reactor for the Si cycle. Extrapolating laboratory-based dissolution experiments performed with pure quartz, Fabre et al. (2019) calculated that the potential flux of dissolution of siliceous sandy beaches that is driven by wave and tidal action. If, according to Luijendijk et al. (2018) one-third of the world's shorelines are sandy beaches, this dissolution flux could be  $3.2 (\pm 1.0) \text{ Tmol Si yr}^{-1}$ . However, this estimate is not well constrained because it has not been validated by field experiments (Supplement, section 2). Cho et al. (2018), using a  $^{228}\text{Ra}$  inverse model and groundwater dSi/ $^{228}\text{Ra}$  ratios, estimate the total (terrestrial + marine) SGD dSi flux to the ocean to be  $3.8 (\pm 1.0) \text{ Tmol-Si yr}^{-1}$ ; this represents an upper limit value for SGD's contribution to the global ocean dSi cycle. Without systematic data that corroborates the net input of dSi through the circulation of the marine component of SGD (e.g., porewater  $\delta^{30}\text{Si}$ , paired dSi and  $^{228}\text{Ra}$  measurements), we estimate the range of net input of dSi through total SGD as  $0.7 \text{ Tmol-Si yr}^{-1}$  (Rahman et al., 2019) to  $3.8 \text{ Tmol-Si yr}^{-1}$  (Cho et al., 2018), with an average, i.e.  $F_{\text{GW}} = 2.3 (\pm 1.1) \text{ Tmol-Si yr}^{-1}$ , which is approximately three times larger than Tréguer & De La Rocha (2013).

#### 2.4 (Sub)polar glaciers ( $F_{\text{ISMW}}$ )

This flux was not considered by Tréguer & De La Rocha (2013). Several researchers have now identified polar glaciers as sources of Si to marine environments (Tréguer, 2014; Meire et al., 2016; Hawkings et al., 2017). The current best estimate of discharge weighted dSi concentration in (sub)Arctic glacial meltwater rivers lies between 20-30  $\mu\text{M}$  although concentrations ranging between 3 and 425  $\mu\text{M}$  have been reported (Graly et al., 2014; Meire et al., 2016; Hatton et al., 2019). Only two values currently exist for dSi from subglacial meltwater beneath the Antarctic Ice Sheet (Whillans Subglacial Lake and Mercer Subglacial Lake, 126 – 140  $\mu\text{M}$ ; Michaud et al., 2016, Hawkings et al., in press), and a limited dataset from periphery glaciers in the McMurdo Dry Valleys and Antarctic Peninsula (~10 – 120  $\mu\text{M}$ ; Hatton et al., 2020; Hirst et al., 2020). Furthermore, iceberg dSi concentrations remain poorly quantified but are expected to be low (~5  $\mu\text{M}$ ) (Meire et al., 2016). Meltwater typically contains high suspended sediment concentrations, due to intense physical erosion by glaciers, with a relatively high dissolvable aSi component (0.3-1.5% dry weight) equating to concentrations of 70-340  $\mu\text{M}$  (Hawkings, 2018; Hatton et al., 2019). Iceberg aSi concentrations are lower (28-83  $\mu\text{M}$ ) (Hawkings et al., 2017). This particulate phase appears fairly soluble in seawater (Hawkings et al., 2017) and large benthic dSi fluxes in glacially influenced shelf seas have been observed (Hendry et al., 2019; Ng et al., 2020). Direct silicic acid input from (sub)polar glaciers is estimated to be 0.04 ( $\pm 0.04$ ) Tmol-Si  $\text{yr}^{-1}$ . If the aSi flux is considered then this may provide an additional 0.29 ( $\pm 0.22$ ) Tmol-Si  $\text{yr}^{-1}$ , with a total  $F_{\text{ISMW}}$  (= dSi+aSi) input estimate of 0.33 ( $\pm 0.26$ ) Tmol-Si  $\text{yr}^{-1}$ . This does not include any additional flux from benthic processing of glacially derived particles in the coastal regions (see section 2.2 above).

## 2.5 Hydrothermal activity ( $F_{\text{H}}$ )

Tréguer & De La Rocha (2013)'s estimate for  $F_{\text{H}}$  was 0.6 ( $\pm 0.4$ ) Tmol-Si  $\text{yr}^{-1}$ . Seafloor hydrothermal activity at mid-ocean ridges (MOR) and ridge-flanks is one of the fundamental processes controlling the exchange of heat and chemical species between seawater and ocean crust (Wheat & Mottl, 2000). A major challenge limiting our current models of both heat and mass flux (e.g. Si flux) through the seafloor is estimating the distribution of the various forms of hydrothermal fluxes, including focused (i.e. high-temperature) vs. diffuse (i.e. low temperature) and ridge axis vs. ridge flank fluxes. Estimates of the Si flux for each input are detailed below.

*Axial and near axial hydrothermal fluxes settings:* The best estimate of the heat flux at ridge axis (i.e. crust 0–0.1 Ma in age) is 1.8 ( $\pm 0.4$ ) TW, while the heat flux in the near-axial region

(i.e. crust 0.1–1 Ma in age) has been inferred at  $1.0 (\pm 0.5)$  TW (Mottl, 2003). The conversion of heat flux to hydrothermal water and chemical fluxes requires assumptions regarding the temperature at which this heat is removed. For an exit temperature of  $350 (\pm 30)^{\circ}\text{C}$  typical of black smoker vent fluids, and an associated enthalpy of  $1,500 (\pm 190) \text{ J g}^{-1}$  at 450–1000 bars and heat flux of  $2.8 (\pm 0.4)$  TW, the required seawater flux is  $5.9 (\pm 0.8) \cdot 10^{16} \text{ g yr}^{-1}$  (Mottl, 2003). High temperature hydrothermal dSi flux is calculated using a dSi concentration of  $19 (\pm 11) \text{ mmol kg}^{-1}$ , which is the average concentration in hydrothermal vent fluids that have an exit temperature  $> 300^{\circ}\text{C}$  (Mottl, 2012). This estimate is based on a compilation of  $> 100$  discrete vent fluid data, corrected for seawater mixing (i.e. end-member values at  $\text{Mg}=0$ , Edmond et al., 1979) and phase separation. Although the chlorinity of hot springs varies widely, nearly all of the reacted fluid, whether vapor or brine, must eventually exit the crust within the axial region. The integrated hot spring flux must therefore have a chlorinity similar to that of seawater. The relatively large range of dSi concentrations in high-temperature hydrothermal fluids likely reflect the range of geological settings (e.g. fast- and slow-spreading ridges) and host-rock composition (ultramafic, basaltic or felsic rocks). Because dSi enrichment in hydrothermal fluids result from mineral-fluid interactions at depth, and is mainly controlled by the solubility of secondary minerals such as quartz (Mottl 1983; Von Damm et al. 1991), it is also possible to obtain a theoretical estimate of the concentration of dSi in global hydrothermal vent fluids. Under the conditions of temperature and pressure (i.e. depth) corresponding to the base of the upflow zone of high temperature ( $>350 - 450^{\circ}\text{C}$ ) hydrothermal systems, dSi concentrations between 16 to 22  $\text{mmol kg}^{-1}$  are calculated, which is in good agreement with measured values in end-member hydrothermal fluids. Using a dSi concentration of  $19 (\pm 3.5) \text{ mmol kg}^{-1}$  and water flux of  $4.8 (\pm 0.8) \cdot 10^{16} \text{ g yr}^{-1}$ , we determine an axial hydrothermal Si flux of  $0.91 (\pm 0.29) \text{ Tmol-Si yr}^{-1}$ . It should be noted, however, that high-temperature hydrothermal fluids may not be entirely responsible for the transport of all the axial hydrothermal heat flux (Elderfield and Schultz, 1996; Nielsen et al., 2006). Because dSi concentrations in diffuse hydrothermal fluids is not significantly affected by subsurface Si precipitation during cooling of the hydrothermal fluid (Escoube et al., 2015), we propose that that the global hydrothermal Si flux is not strongly controlled by the nature (focused vs. diffuse) of axial fluid flow.

*Ridge flank hydrothermal fluxes:* Chemical fluxes related to seawater-crust exchange at ridge flanks has been previously determined through direct monitoring of fluids from low-temperature hydrothermal circulation (Wheat and Mottl, 2000). Using basaltic formation fluids from the 3.5 Ma crust on the eastern flank of the Juan de Fuca Ridge (Wheat and McManus,



2005), a global flux of  $0.011 \text{ Tmol-Si yr}^{-1}$  for warm ridge flank is calculated. This estimate is based on the measured Si anomaly associated with warm spring ( $0.17 \text{ mmol kg}^{-1}$ ) and a ridge flank fluid flux determined using oceanic Mg mass balance, therefore assuming that the ocean is at steady-state with respect to Mg. More recent results of basement fluid compositions in cold and oxygenated ridge flank settings (e. g. North Pond, Mid-Atlantic Ridge) also confirms that incipient alteration of volcanic rocks may result in significant release of Si to circulating seawater (Meyer et al., 2016). The total heat flux through ridge flanks, from 1 Ma crust to a sealing age of 65 Ma, has been estimated at  $7.1 (\pm 2) \text{ TW}$ . Considering that most of ridge-flank hydrothermal power output should occur at cool sites ( $< 20^\circ\text{C}$ ), the flux of slightly altered seawater could range from  $0.2$  to  $2 \times 10^{19} \text{ g yr}^{-1}$ , rivaling with the flux of river water to the ocean of  $3.8 \times 10^{19} \text{ g yr}^{-1}$  (Mottl, 2003). Using this estimate and Si anomaly of  $0.07 \text{ mmol-Si kg}^{-1}$  reported in cold ridge flank setting from North Pond (Meyer et al., 2016), a Si flux of  $0.14$  to  $1.4 \text{ Tmol-Si yr}^{-1}$  for cold ridge flank could be calculated. Because of the large volume of seawater interacting with oceanic basalts in ridge flank settings, even a small chemical anomaly resulting from reactions within these cold systems could result in a globally significant elemental flux. Hence, additional studies are required to better determine the importance of ridge flanks to oceanic Si budget.

Combining axial and ridge flank estimates, the best estimate for  $F_H$  is now  $1.7 (\pm 0.8) \text{ Tmol-Si yr}^{-1}$ , approximately three times larger than the estimate from Tréguer & De La Rocha (2013).

## 2.6 Total net inputs (Table 1A)

Total Si input =  $8.1 (\pm 2.0) (F_{R(dSi+asSi)}) + 0.5 (\pm 0.5) (F_A) + 1.9 (\pm 0.7) (F_W) + 2.3 (\pm 1.1) (F_{GW}) + 0.3 (\pm 0.3) (F_{ISMW}) + 1.7 (\pm 0.8) (F_H) = 14.8 (\pm 2.6) \text{ Tmol-Si yr}^{-1}$ .

The uncertainty of the total Si inputs (and total Si outputs, section 3) has been calculated using the error propagation method from Bevington and Robinson (2003). This has been done for both the total fluxes and the individual flux estimates.

## 3. Advances in output fluxes

### 3.1 Long-term burial of planktonic biogenic silica in sediments ( $F_B$ )

Long-term burial of bSi, which generally occurs below the top 10-20 cm of sediment, was estimated by Tréguer & De La Rocha (2013) to be  $6.3 (\pm 3.6) \text{ Tmol-Si yr}^{-1}$ . The burial rates are highest in the Southern Ocean (SO), the North Pacific Ocean, the equatorial Pacific Ocean, and in the coastal and continental margin zone (CCMZ; DeMaster et al., 2002; Hou et al., 2019; Rahman et al., 2017).

279 Post-depositional redistribution by processes like winnowing or focusing by bottom currents  
 280 can lead to under- and over-estimation of uncorrected sedimentation and burial rates. To correct  
 281 for these processes, the burial rates are typically normalized using the particle reactive nuclide  
 282  $^{230}\text{Th}$  method (e.g. Geibert et al., 2005). A  $^{230}\text{Th}$  normalization of bSi burial rates has been  
 283 extensively used for the SO (Tréguer and De La Rocha, 2013), particularly in the “opal belt”  
 284 zone (Pondaven et al., 2000; DeMaster, 2002; Geibert et al., 2005). Chase et al. (2015) re-  
 285 estimated the SO burial flux, south of  $40^\circ\text{S}$ , at  $2.3 (\pm 1.0) \text{ Tmol-Si yr}^{-1}$ .  
 286 Hayes et al. (pers. comm., Hayes et al. under review) recently calculated total marine bSi burial  
 287 of  $5.46 (\pm 1.18) \text{ Tmol-Si yr}^{-1}$ , using a database that comprises 2,948 bSi concentrations of top  
 288 core sediments and  $^{230}\text{Th}$ -corrected accumulation fluxes of open ocean locations  $>1 \text{ km}$  in  
 289 depth. Hayes et al.’s  $^{230}\text{Th}$ -corrected total burial rate is  $2.68 (\pm 0.61) \text{ Tmol-Si yr}^{-1}$  south of  $40^\circ\text{S}$ ,  
 290 close to Chase et al. (2015)’s estimate for the SO. Hayes et al. do not distinguish between the  
 291 different analytical methods used for the determination of the bSi concentrations of these 2948  
 292 samples to calculate total bSi burial. These methods include alkaline digestion methods (with  
 293 variable protocols for correcting from lithogenic interferences e.g. DeMaster, 1981; Mortlock  
 294 and Froelich, 1989; Müller and Schneider, 1993), X-ray diffraction (e.g. Leinen et al., 1986),  
 295 X-ray fluorescence (e.g. Finney et al., 1988), Fourier-transform infra-red spectroscopy  
 296 (Lippold et al, 2012), and inductively coupled plasma mass spectrometry (e.g. Prakash Babu et  
 297 al., 2002). An international exercise calibration on the determination of bSi concentrations of  
 298 various sediments (Conley, 1998) concluded that the X-ray diffraction (XRD) method  
 299 generated bSi concentrations that were on average 24% higher than the alkaline digestion  
 300 methods. In order to test the influence of the XRD method on their re-estimate of total bSi  
 301 burial, Hayes et al. found that their re-estimate ( $5.46 (\pm 1.18) \text{ Tmol-Si yr}^{-1}$ ), which includes  
 302 XRD data (~40% of the total number of data points), did not differ significantly from a re-  
 303 estimate that does not include XRD data points ( $5.43 (\pm 1.18) \text{ Tmol-Si yr}^{-1}$ ). As a result, this  
 304 review includes Hayes et al.’s re-estimate for the open-ocean annual burial rate, i.e.  $5.5 (\pm 1.2)$   
 305  $\text{Tmol-Si yr}^{-1}$ .  
 306 The best estimate for the open-ocean total burial now becomes  $2.8 (\pm 0.6) \text{ Tmol-Si yr}^{-1}$  without  
 307 the SO contribution ( $2.7 (\pm 0.6) \text{ Tmol-Si yr}^{-1}$ ). This value is an excess of  $1.8 \text{ Tmol-Si yr}^{-1}$  over  
 308 the DeMaster (2002) and Tréguer and De La Rocha (2013) estimates, which were based on 31  
 309 sediment cores mainly distributed in the Bering Sea, the North Pacific, the Sea of Okhotsk, and  
 310 the Equatorial Pacific (total area  $23 \text{ M km}^2$ ), and where bSi% was determined solely using  
 311 alkaline digestion methods.

Estimates of the silica burial rates have been usually determined from carbon burial rates using a Si:C ratio of 0.6 in CCMZ (DeMaster 2002). However, we now have independent estimates of marine organic C and total initial bSi burial (e.g. Aller et al., 1996; Aller et al., 2008; Galy et al., 2007; Rahman et al., 2016, 2017). It has been shown that the initial bSi burial in sediment evolved as unaltered bSi or as authigenically formed alumino-silicate phases (Rahman et al., 2017). The Si:C burial ratios of residual marine plankton post-remineralization in tropical and subtropical deltaic systems are much greater (2.4 - 11) than the 0.6 Si:C burial ratio assumed for continental margin deposits (DeMaster, 2002). The sedimentary Si:C preservation ratios are therefore suggested to depend on differential remineralization pathways of marine bSi and  $C_{org}$  under different diagenetic regimes (Aller, 2014). Partitioning of  $^{32}Si$  activities between bSi and mineral pools in tropical deltaic sediments indicate rapid and near-complete transformation of initially deposited bSi to authigenic clay phases (Rahman et al., 2017). For example, in subtropical/temperate deltaic and estuarine deposits  $^{32}Si$  activities signal represent approximately ~50% of initial bSi<sub>opal</sub> delivery to sediments (Rahman et al., 2017). Using the  $^{32}Si$  technique Rahman et al. (2017) provided an updated estimate of bSi burial for the CCMZ of  $3.7 (\pm 2.1) \text{ Tmol-Si yr}^{-1}$ , higher than the Tréguer and De La Rocha (2013) estimate of  $3.3 (\pm 2.1) \text{ Tmol-Si yr}^{-1}$  based on the Si:C method of DeMaster (2002).

Combining the Hayes et al. (in review) burial rate for the open ocean zone including the SO, and the Rahman et al. (2017) estimate for the CCMZ gives a revised global total burial flux,  $F_B$ , of  $9.2 (\pm 1.6) \text{ Tmol-Si yr}^{-1}$ , 46% larger than the Tréguer and De La Rocha (2013) estimate.

### **3.2 Deposition and long-term burial of sponge silica ( $F_{SP}$ )**

Tréguer and De La Rocha (2013)'s estimate for  $F_{SP}$ , the net sink of sponge bSi in sediments of continental margins, was  $3.6 (\pm 3.7) \text{ Tmol Si yr}^{-1}$ . The longevity of sponges, ranging from years to millennia, temporally decouples the process of skeleton production from the process of deposition to the sediments (Jochum et al., 2017). While sponges slowly accumulate bSi over their long and variable lifetimes (depending on the species), the deposition to the sediments of the accumulated bSi is a relatively rapid process after sponge death, lasting days to months (Supplement, section 3). Tréguer and De La Rocha (2013)'s estimate was calculated as the difference between the sponge dSi demand on continental shelves ( $3.7 (\pm 3.6) \text{ Tmol Si yr}^{-1}$ ) — estimated from silicon consumption rates available for few sublittoral sponge species (Maldonado et al., 2011) —, and the flux of dSi from the dissolution of sponge skeletons in continental shelves ( $0.15 (\pm 0.15) \text{ Tmol Si yr}^{-1}$ ). This flux was tentatively estimated from the rate of dSi dissolution from a rare, unique glass sponge reef at British Columbia (Canada) (Chu et al., 2011) and which is unlikely to be representative of the portion of sponge bSi that dissolves

back as dSi after sponge death and before their burial in the sediments. To improve the estimate, Maldonado et al. (2019) used microscopy to access the amount of sponge silica that was actually being buried in the marine sediments using 17 sediment cores representing different marine environments. The deposition of sponge bSi was found to be one order of magnitude more intense in sediments of continental margins and seamounts than on continental rises and central basin bottoms. The new best estimate for  $F_{SP}$  is  $1.7 (\pm 1.6) \text{ Tmol-Si yr}^{-1}$ , assuming that the rate of sponge silica deposition in each core was approximately constant through the Holocene, i.e. two times smaller than Tréguer and De La Rocha's preliminary estimate.

### 3.3 Reverse Weathering flux ( $F_{RW}$ )

The previous estimate for this output flux, provided by Tréguer & De La Rocha (2013),  $F_{RW} = 1.5 (\pm 0.5) \text{ Tmol-Si yr}^{-1}$ , was determined using indirect evidence since the influence of reverse weathering on the global Si cycle prior to 2013 was poorly understood. For example, reverse weathering reactions at the sediment–water interface were previously thought to constitute a relatively minor sink ( $0.03 - 0.6 \text{ Tmol-Si yr}^{-1}$ ) of silica in the ocean (DeMaster, 1981). The transformation of bSi to a neoformed aluminosilicate phase, or authigenic clay formation, was assumed to proceed slowly ( $> 10^4 - 10^5$  years) owing principally to the difficulty of distinguishing the contribution of background lithogenic or detrital clays using the common leachates employed to quantify bSi (DeMaster, 1981). Recent direct evidence supporting the rapid formation of authigenic clays comes from tropical and subtropical deltas (Michalopoulos & Aller, 1995; Rahman et al., 2016, 2017; Zhao et al., 2017) and several geochemical tools show that authigenic clays may form ubiquitously in the global ocean (Baronas et al., 2017; Ehlert et al., 2016a; Geilert et al., 2020; Michalopoulos & Aller, 2004; Pickering et al., 2020). Activities of cosmogenic  $^{32}\text{Si}$  ( $t_{1/2} \sim 140$  yrs), incorporated into bSi in the surface ocean, provide demonstrable proof of rapid reverse weathering reactions by tracking the fate of bSi upon delivery to marine sediments (Rahman et al., 2016). By differentiating sedimentary bSi storage between unaltered bSi ( $b\text{Si}_{opal}$ ) and diagenetically altered bSi ( $b\text{Si}_{altered}$ ) in the proximal coastal zone,  $^{32}\text{Si}$  activities in these pools indicate that  $3.7 \text{ Tmol-Si yr}^{-1}$  is buried as unaltered  $b\text{Si}_{opal}$  and  $4.7 (\pm 2.3) \text{ Tmol-Si yr}^{-1}$  as authigenic clays ( $b\text{Si}_{clay}$ ) on a global scale. Here, we adopt  $4.7 \text{ Tmol-Si yr}^{-1}$  for  $F_{RW}$  representing about three times the Tréguer & De La Rocha (2013)'s value.

### 3.4 Total net output (Table 1A)

Total Si output =  $9.2 (\pm 1.6) (F_{B(net\ deposit)}) + 4.7 (\pm 2.3) (F_{RW}) + 1.7 (\pm 1.6) (F_{SP}) = \mathbf{15.6 (\pm 2.4) \text{ Tmol-Si yr}^{-1}}$ .

## 4. Advances in biological fluxes

## **4.1 bSi annual pelagic production**

### **4.1.1 from field data**

The last evaluation of global marine silica production was by Nelson et al. (1995) who estimated global gross marine bSi pelagic production to be  $240 (\pm 40) \text{ Tmol-Si yr}^{-1}$ . Since 1995, the number of field studies of bSi production (using either the  $^{30}\text{Si}$  tracer method, Nelson & Goering (1977) or the  $^{32}\text{Si}$  method (Tréguer et al., 1991; Brzezinski & Phillips, 1997), has grown substantially from 15 (1995) to 49 in 2019, allowing the first estimate based on empirical silica production rate measurements (Fig. 3, and Supplement, section 4). It is usually assumed that the silica production, as measured using the above methods, is mostly supported by diatoms, with some unknown (but minor) contribution of other planktonic species.

The silica production rates measured during 49 field campaigns were assigned to Longhurst provinces (Longhurst, 2007; Longhurst et al., 1995) based on location, with the exception of the SO, where province boundaries were defined according to Tréguer & Jacques (1992). Extrapolating these “time-and-space-limited” measurements of bSi spatially to a biogeographic province, and annually from the bloom phenology for each province (calculated as the number of days where the chlorophyll concentration is greater than the average concentration between the maximum and the minimum values), results in annual silica production estimates for 26 of the 56 world ocean provinces. The annual production of all provinces in a basin were averaged for the “ocean basin” estimate (Table 2) and then extrapolated by basin area. The averages from provinces were subdivided among coastal for the “domain” estimate (Table 2), SO, and open ocean domains, and extrapolated based on the area of each domain. Averaging the “ocean basin” and the “domain” annual estimates (Table 2), our best estimate for the global marine bSi production is  $267 (\pm 18) \text{ Tmol-Si yr}^{-1}$  (Table 2).

### **4.1.2 bSi annual pelagic production from models**

Estimates of bSi production were also derived from satellite productivity models, and from global ocean biogeochemical models (GOBMs). We used global net primary production (NPP) estimates from the carbon-based productivity model (Westberry et al., 2008) and the vertically generalized productivity model (VGPM) (Behrenfeld & Falkowski, 1997) for the estimates based on satellite productivity models. NPP estimates from these models were divided into oligotrophic ( $< 0.1 \mu\text{g Chl a L}^{-1}$ ), mesotrophic ( $0.1 - 1.0 \mu\text{g Chl a L}^{-1}$ ) and eutrophic ( $> 1.0 \mu\text{g Chl a L}^{-1}$ ) areas (Carr et al., 2006). The fraction of productivity by diatoms in each area was determined using the DARWIN model (Dutkiewicz et al., 2015) allowing a global estimate where diatoms account for 29% of the production. Each category was further subdivided into High Nutrient Low Chlorophyll (HNLC) zones ( $>5 \mu\text{M}$  surface nitrate, Garcia et al., 2014),

coastal zones (< 300 km from a coastline) and open ocean (remainder) zones for application of Si:C ratios to convert to diatom silica production. Si:C ratios were 0.52 for HNLC regions, 0.065 for the open ocean and 0.13 for the coastal regions, reflecting the effect of Fe limitation in HNLC areas (Franck et al., 2000), of Si limitation for uptake in the open ocean (Brzezinski et al., 1998, 2011; Brzezinski & Nelson, 1996; Krause et al., 2012), and of replete conditions in the coastal zone (Brzezinski, 1985). Silica production estimates were then subdivided between coast (within 300 km of shore), open ocean and SO (northern boundary 43°S from Australia to South America, 34.8°S from South America to Australia) and summed to produce regional estimates (Table 2). Our best estimate for the global marine bSi production is 207 ( $\pm$  23) Tmol-Si yr<sup>-1</sup> from satellite productivity models (Table 2).

A second model-based estimate of silica production used 18 numerical GOBMs models of the marine silica cycle that all estimated global silica export from the surface ocean (Aumont et al., 2015; Bernard et al., 2011; De Souza et al. 2014; Dunne et al., 2007; Dutkiewicz et al., 2015; Gnanadesikan et al., 1999; Heinze et al., 2003; Holzer et al., 2014; Jin et al., 2006; Matsumoto et al., 2013; Pasquier & Holzer, 2017; Roshan et al., 2018; Sarmiento et al., 2007; Usbeck, 1999; Ward et al., 2012; Wischmeyer et al., 2003). These include variants of the MOM, HAMOCC OCIM, DARWIN, cGENIE and PICES models. Export production was converted to gross silica production by using a silica dissolution-to-production (D:P) ratio for the surface open ocean of 0.58 and 0.51 for the surface of coastal regions (Tréguer & De La Rocha, 2013). Model results were first averaged within variants of the same model and then averaged across models to eliminate biasing the average to any particular model. Our best estimate from GOBMs for the global marine bSi production is 276 ( $\pm$  23) Tmol-Si yr<sup>-1</sup> (Table 2). Averaging the estimates calculated from satellite productivity models and GOBMs give a value of 242 ( $\pm$  49) Tmol-Si yr<sup>-1</sup> for the global marine bSi production (Table 2).

#### 4.1.3 Best estimate for bSi annual pelagic production

Using a simple average of the “field” and “model” estimates, the revised best estimate of global marine gross bSi production, mostly due to diatoms, is now  $F_{P_{gross}} = 255 (\pm 52) \text{ Tmol-Si yr}^{-1}$ , not significantly different from the Nelson et al. (1995)’s value.

In the SO, a key area for the world ocean Si cycle (DeMaster, 1981), there is some disagreement among the different methods of estimating bSi production. Field studies give an estimate of 67 Tmol-Si yr<sup>-1</sup> for the annual gross production of silica in the SO, close to the estimate of 60 Tmol-Si yr<sup>-1</sup> calculated using satellite productivities models (Table 2). However, the bSi production in the SO estimated by ocean biogeochemical models is about twice as high, at 129 Tmol-Si yr<sup>-1</sup> (Table 2). The existing in-situ bSi production estimates are too sparse to be able

to definitively settle whether the lower estimate or the higher estimate is correct, but there is reason to believe that there are potential biases in both the satellite NPP models and the ocean biogeochemical models. SO chlorophyll concentrations may be underestimated by as much as a factor of 3-4 (Johnson et al., 2013), which affects the NPP estimates in this region and hence our bSi production estimates by this method. The bSi production estimated by ocean biogeochemical models is highly sensitive to vertical exchange rates in the SO (Gnanadesikan and Toggweiler, 1999), and is also dependent on the representation of phytoplankton classes in models with explicit representation of phytoplankton. Models that have excessive vertical exchange in the SO (Gnanadesikan and Toggweiler, 1999), or that represent all large phytoplankton as diatoms, may overestimate the Si uptake by plankton in the SO. Other sources of uncertainty in our bSi production estimates include poorly-constrained estimates of the Si:C ratio and dissolution:production ratios (see Supplement section 4). The errors incurred by these choices are more likely to cancel out in the global average, but could be significant at regional scales, potentially contributing to the discrepancies in SO productivity across the various methods.

#### 4.1.4 Estimates of the bSi production of other pelagic organisms

Extrapolations from field and laboratory work show that the contribution of picocyanobacteria (like *Synechococcus*, Baines et al. 2012, Brzezinski et al., 2017; Krause et al., 2017) to the world ocean accumulation of bSi is  $< 20 \text{ Tmol-Si yr}^{-1}$ . The gross silica production of rhizarians, siliceous protists, in the 0-1000 m layer might range between  $2 - 58 \text{ Tmol-Si yr}^{-1}$ , about 50% of it occurring in the 0-200 m layer (Llopis Monferrer et al., 2020).

Note that these preliminary estimates of bSi accumulation or production by picocyanobacteria and rhizarians are within the uncertainty of our best estimate of  $F_{\text{Pgross}}$ .

#### 4.2 Estimates of the bSi production of benthic organisms

The above updated estimate of the pelagic production does not take into account bSi production by benthic organisms like benthic diatoms and sponges. Our knowledge of the production terms for benthic diatoms is poor and no robust estimate is available for bSi annual production of benthic diatoms at global scale (Supplement, section 4).

Substantial progress has been made for silica deposition by siliceous sponges recently. Laboratory and field studies reveal that sponges are highly inefficient in the molecular transport of dSi compared to diatoms and consequently bSi production, particularly when dSi concentrations are lower than  $75 \mu\text{M}$ , a situation that applies to most ocean areas (Maldonado et al., 2020). On average, sponge communities are known to produce bSi at rates that are about 2 orders of magnitude smaller than those measured for diatom communities (Maldonado et al.,

2012). The global standing crop of sponges is very difficult to be constrained and the annual bSi production attained by such standing crop even more difficult to estimate because sponge populations are not homogeneously distributed on the marine benthic environment and extensive, poorly mapped and unquantified aggregations of heavily silicified sponges occur in deep sea of all oceans. A first tentative estimate of bSi production for sponges on continental shelves, where sponge biomass can be more easily approximated, ranged widely, from 0.87 to 7.39 Tmol-Si yr<sup>-1</sup>, because of persisting uncertainties in estimating sponge standing crop (Maldonado et al., 2012). A way to estimate the global annual bSi production by sponges without knowing their standing crop is to retrace bSi production values from the amount of sponge bSi that is annually being deposited to the ocean bottom, after assuming that, in the long run, the standing crop of sponges in the ocean is in equilibrium (i.e, it is neither progressively increasing nor decreasing over time). The deposition rate of sponge bSi has been estimated at 49.95 (± 74.14) mmol-Si m<sup>-2</sup> yr<sup>-1</sup> on continental margins, at 0.44 (± 0.37) mmol-Si m<sup>-2</sup> yr<sup>-1</sup> in sediments of ocean basins where sponge aggregations do not occur and at 127.30 (± 105.69) mmol-Si m<sup>-2</sup> yr<sup>-1</sup> in deep-water sponge aggregations (Maldonado et al., 2019). A corrected sponge bSi deposition rate for ocean basins is estimated at 2.98 (± 1.86) mmol Si m<sup>-2</sup> yr<sup>-1</sup> assuming that sponge aggregations do not occupy more than 2% of seafloor of ocean basins (Maldonado et al., 2019). A total value of 6.15 (± 5.86) Tmol-Si yr<sup>-1</sup> can be estimated for the global ocean when the average sponge bSi deposition rate for continental margins and seamounts (representing 108.02 Mkm<sup>2</sup> of seafloor) and for ocean basins (253.86 Mkm<sup>2</sup>) is scaled up through the extension of those bottom compartments. If the bSi production being accumulated as standing stock in the living sponge populations annually is assumed to become constant in a long-term equilibrium state, the global annual deposition rate of sponge bSi can be considered as a reliable estimate of the minimum value that the annual bSi production by the sponges can reach in the global ocean. The large associated SD value does not derive from the approach being unreliable but from the spatial distribution of the sponges on the marine bottom being extremely heterogeneous, with some ocean areas being very rich in sponges and sponge bSi in sediments at different spatial scales while other areas are completely deprived from these organisms.

## 5. Discussion

### 5.1 Overall residence times

The overall geological residence time for Si in the ocean ( $\tau_G$ ) is equal to the total amount of dSi in the ocean divided by the net input (or output) flux. We re-estimate the total ocean dSi



inventory value derived from the Pandora model (Peng et al. 1993), which according to Tréguer et al. (1995) was 97,000 Tmol-Si. An updated estimate of the global marine dSi inventory was computed by interpolating the objectively analyzed annual mean silicate concentrations from the 2018 World Ocean Atlas (Garcia et al., 2019) to the OCIM model grid (Roshan et al., 2018). Our estimate is now 120,000 Tmol-Si, i.e. about 24 % higher than the Tréguer et al. (1995) estimate. Tables 1B and 3 show updated estimates of  $\tau_G$  from Tréguer et al. (1995) and Tréguer & De La Rocha (2013) using this updated estimate of the total dSi inventory into account. Our updated budget (Fig. 1, Table 1B, Table 3A) reduces past estimates of  $\tau_G$  (Tréguer et al., 1995; Tréguer and De La Rocha, 2013) by more than half, from ca.18 kyr to ca. 8 kyr (Table 3C). This brings the ocean residence time of Si closer to that of nitrogen (< 3 kyr, Sarmiento & Gruber, 2006) than phosphorus (30 – 50 kyr, Sarmiento & Gruber, 2006).

The overall biological residence time,  $\tau_B$ , is calculated by dividing the total dSi content of the world ocean by gross silica production. It is calculated from the bSi pelagic production only given the large uncertainty on our estimate of the bSi production by sponges.  $\tau_B$  is ca. 470 years (Table 1B, Table 3). Thus, Si delivered to the ocean passes through the biological uptake and dissolution cycle on average 16 times ( $\tau_G / \tau_B$ ) before being removed to the sea floor (Table 1B, Table 3C).

The new estimate for the global average preservation efficiency of bSi buried in sediments is ( $F_B = 9.2 / F_{P_{gross}} = 255$ ) 3.6 %, similar to the Tréguer and De La Rocha (2013) estimate, making bSi in sediments an intriguing potential proxy for export production (Tréguer et al., 2018). Note that the reverse weathering flux ( $F_{RW}$ ) is also fed by the export flux ( $F_E$ ), (Fig. 4). So, the preservation ratio of biogenic silica in sediment can be calculated as  $F_B + F_{RW} / F_{P_{gross}} = 13.9 / 255 = 5.45\%$ , which is ~30 times larger than the carbon preservation efficiency.

## 5.2 The issue of steady state

Over a given time scale, an elemental cycle is at steady state if the outputs balance the inputs in the ocean and the mean concentration of the dissolved element remains constant.

### 5.2.1 Long time scales ( $>\tau_G$ )

Over geologic time scales, the average dSi concentration of the ocean has undergone drastic changes. A seminal work (Siever, 1991) on the biological – geochemical interplay of the Si cycle showed a factor of 100 decline in ocean dSi concentration from 550 Myr to the present. This decline was marked by the rise of silicifiers like radiolarian and sponges during the Phanerozoic. Then during the mid-Cenozoic diatoms started to dominate a Si cycle previously controlled by inorganic and diagenetic processes. Conley et al., (2017) hypothesized that biological processes might also have influenced the dSi concentration of the ocean at the start

550 of oxygenic photosynthesis taking into account the impact of the evolution of biosilicifying  
 551 organisms (including bacterial-related metabolism). There ~~is~~ further evidence that the existing  
 552 lineages of sponges have their origin in ancient (Mesozoic) oceans with much higher dSi  
 553 concentrations than the modern ocean. Some recent sponge species can only complete their  
 554 silica skeletons if dSi concentration much higher than those in their natural habitat are provided  
 555 experimentally (Maldonado et al., 1999). Also, all recent sponge species investigated to date  
 556 have kinetics of dSi consumption that reach their maximum speed only at dSi concentrations  
 557 that are one to two orders of magnitude higher than the current dSi availability in the sponge  
 558 habitats, indicating that the sponge physiology evolved in dSi-rich, ancestral scenarios. Note  
 559 that with a geological residence time of Si of ca. 8,000 years, the Si cycle can fluctuate over  
 560 glacial-interglacial time scale.

#### 561 **5.2.2 Short time scales ( $< \tau_G$ )**

562 In the modern ocean the main control over silica burial and authigenic formation rate is the bSi  
 563 production rate of pelagic and benthic silicifiers, as shown above. The gross production of bSi  
 564 due to diatoms depends on the dSi availability in the surface layer (Fig. 1). Silicic acid does not  
 565 appear to be limiting in several zones of the world ocean, which include the coastal zones, and  
 566 the HNLC zones (Tréguer & De La Rocha, 2013). Note that any short-term change of dSi inputs  
 567 does not imply modification of bSi production, nor export, nor burial rate. For this reason,  
 568 climatic changes or anthropogenic impacts that affect dSi inputs to the ocean by rivers and/or  
 569 other pathways, could lead to an imbalance of Si inputs and outputs in the modern ocean.

#### 570 **5.2.3 A possible steady-state scenario**

571 Within the limits of uncertainty, the total net inputs of dSi and aSi are  $14.8 (\pm 2.6)$  Tmol-Si yr<sup>-1</sup>  
 572 and are approximately balanced by the total net output flux of Si of  $15.6 (\pm 2.4)$  Tmol-Si yr<sup>-1</sup>.  
 573 Fig. 1 supports the hypothesis that the modern ocean Si cycle is at steady state, compatible with  
 574 the geochemical and biological fluxes of Table 1.

575 Consistent with Fig. 1, Fig. 4 shows a steady-state scenario for the Si cycle in the coastal and  
 576 continental margins zone (CCMZ), often called the “boundary exchange” zone which,  
 577 according to Jeandel (2016) and Jeandel & Oelkers (2015), plays a major role in the land-to-  
 578 ocean transfer of material (also see Fig. 2). Fig. 4 illustrates the interconnection between  
 579 geochemical and biological Si fluxes, particularly in the CCMZ. In agreement with Laruelle et  
 580 al. (2009), Fig. 4 also shows that the “open ocean” bSi production is mostly fueled by dSi inputs  
 581 from below ( $92.5$  Tmol-Si yr<sup>-1</sup>) and not by the CCMZ ( $4.7$  Tmol-Si yr<sup>-1</sup>) (Supplemental section  
 582 5).

### 583 **5.3 The impacts of global change on the Si cycle**

Supprimé: are

As illustrated by Fig. 1 and 4, the pelagic bSi production is mostly fueled from the large, deep ocean recycled pool of dSi. This lengthens the response time of the Si cycle to changes in dSi inputs to the ocean due to global change (including climatic and anthropogenic effects), increasing the possibility for the Si cycle to be out of balance.

### **5.3.1 Impacts on riverine inputs of dSi and aSi**

Climate change at short time scale during the 21<sup>st</sup> century impacts the ocean delivery of riverine inputs of dSi and aSi ( $F_R$ ) and of the terrestrial component of the submarine groundwater discharge ( $F_{GW}$ ), either directly (e.g. dSi and aSi weathering and transport), or indirectly by affecting forestry and agricultural dSi export. So far the impacts of climate change on the terrestrial Si cycle have been reported for boreal wetlands (Struyf et al., 2010), North American (Opalinka & Cowling, 2015) and western Canadian Arctic rivers (Phillips, 2020), and the tributaries of the Laptev and East Siberian Seas (Charette et al., 2020), but not for tropical environments. Tropical watersheds are the key areas for the transfer of terrestrial dSi to the ocean, as approximately 74% of the riverine Si input is from these regions (Tréguer et al., 1995). Precipitation in tropical regions usually follow “the rich-get-richer” mechanism in a warming climate according to model predictions (Chou et al., 2004, 2008). In other words, in tropical convergence zones rainfall increases with climatological precipitation, but the opposite is true in tropical subsidence regions, creating diverging impacts for the weathering of tropical soils. If predictions of global temperature increase and variations in precipitations of the IPCC are correct (IPCC, 2018) it is uncertain how  $F_R$  or  $F_{GW}$ , two major components of dSi and aSi inputs, will change. Consistent with these considerations are the conclusions of Phillips (2020) on the impacts of climate change on the riverine delivery of dSi to the ocean, using machine-learning based approach. Phillips (2020) predicts that within the end of this century dSi mean yield could increase regionally (for instance in the Arctic region), but the global mean dSi yield is projected to decrease, using a model based on 30 environmental variables including temperature, precipitation, land cover, lithology, and terrain.

### **5.3.2 Abundance of marine and pelagic and benthic silicifiers**

A change in diatom abundance was not seen on the North Atlantic from Continuous Plankton Recorder (CPR) data over the period 1960-2009 (Hinder et al., 2012). However, studies have cautioned that many fields (e.g. Chl) will take several decades before these changes can be measured precisely beyond natural variability (Henson et al 2010; Dutkiewicz et al 2019). The melting of Antarctic ice platforms has already been noticed to trigger impressive population blooms of highly silicified sponges (Fillinger et al. 2013).

### **5.3.3. Predictions for the ocean phytoplankton production and bSi production**

619 Twenty-first century climate change will affect ocean circulation, stratification and upwelling,  
 620 and therefore nutrient cycling (Aumont et al., 2003; Bopp et al., 2005, 2013). With increased  
 621 stratification dSi supply from upwelling will reduce (Fig. 1 and 4) leading to less siliceous  
 622 phytoplankton production in surface compartments of lower latitudes and possibly the North  
 623 Atlantic (Tréguer et al., 2018). The impact of climate change on the phytoplankton production  
 624 in polar seas is highly debated as melting of sea ice decreases light limitation. In the Arctic  
 625 Ocean an increase in nutrient supply from river- and shelf derived waters (at the least for silicic  
 626 acid) will occur through the Transpolar Drift potentially impacting rates of primary production,  
 627 including bSi production (e.g. Charette et al., 2020). In the SO bSi production may increase in  
 628 the coastal and continental shelf zone as iron availability increases due to ice sheet melt and  
 629 iceberg delivery (Duprat et al., 2016; Herraiz-Borreguero et al., 2016; Boyd et al., 2016;  
 630 Hutchins & Boyd, 2016; Tréguer et al., 2018; Hawkings et al., in press). However, Henley et al  
 631 (2019) suggests a shift from diatoms to haptophytes and cryptophytes with changes in ice  
 632 coverage in the Western Antarctic Peninsula. How such changes in coastal environments and  
 633 nutrient supplies will interplay is unknown. Globally, it is very likely that a warmer and more  
 634 acidic ocean alters the pelagic bSi production rates, thus modifying the export production and  
 635 outputs of Si at short time scales.

636 Although uncertainty is substantial, modelling studies (Bopp et al., 2005; Dutkiewicz et al.,  
 637 2019; Laufkötter et al, 2015) suggest regional shifts in bSi pelagic production with climatic  
 638 change. These models predict a global decrease in diatom biomass and productivity over the  
 639 the 21<sup>st</sup> century (Bopp et al., 2005, Dutkiewicz et al., 2019, Laufkötter et al., 2015), which  
 640 would lead to a reduction in the pelagic biological flux of silica. Regional responses differ, with  
 641 most models suggesting a decrease in diatom productivity in the lower latitudes and many  
 642 predicting an increase in diatom productivity in the SO (Laufkötter et al, 2015). Holzer et al.  
 643 (2019) suggest that changes in supply of dFe will alter bSi production mainly by inducing  
 644 floristic shifts, not by relieving kinetic limitation. Increased primary productivity is predicted  
 645 to come from a reduction in sea-ice area, faster growth rates in warmer waters and longer  
 646 growing seasons in the high latitudes. However, many models have very simple ecosystems  
 647 including only diatoms and a small phytoplankton. In these models, increased primary  
 648 production in the SO is mostly from diatoms. Models with more complex ecosystem  
 649 representations (i.e. including additional phytoplankton groups) suggest that increased primary  
 650 productivity in the future SO will be due to other phytoplankton types (e.g. pico-eukaryote) and  
 651 that diatoms biomass will decrease (Dutkiewicz et al, 2019; also see model PlankTOM5.3 in  
 652 Laufkötter et al, 2015), except in regions where sea-ice cover has reduced. Differences in the

complexity of the ecosystem and parameterizations, in particular in terms of temperature dependences of biological process, between models lead to widely varying predictions (Dutkiewicz et al., 2019; Laufkotter et al., 2015). These uncertainties suggest we should be cautious in our predictions of what will happen with the silica biogeochemical cycle in a future ocean.

### 5.5 Other anthropogenic impacts

For decades if not centuries, anthropogenic activities directly or indirectly altered the Si cycle in rivers, and the CCMZ (Bernard et al., 2010; Conley et al. 1993; Derry et al. 2005; Humborg et al., 2006; Ittekkot et al., 2000, 2006; Laruelle et al. 2009; Liu et al., 2012; Yang et al., 2015; Wang et al., 2018; Zhang et al., 2019). Processes involved include eutrophication and pollution (Conley et al., 1993; Liu et al., 2012), river damming (Ittekkot, 2006; Ittekkot et al., 2000; Yang et al., 2015; Wang et al., 2018), deforestation (Conley, 2008), changes in weathering and in river discharge (Bernard et al. 2010; Yang et al. 2015), and deposition load in river deltas (Yang et al., 2015).

Among these processes, river damming is known for having the most spectacular and short time-scale impacts on the Si delivery to the ocean. River damming favours enhanced biologically mediated absorption of dSi in the dam reservoir, thus resulting in significant decreases in dSi concentration downstream. Drastic perturbations on the Si-cycle and downstream ecosystem have been shown (Ittekkot, 2006; Ittekkot et al. 2000; Humborg et al. 2006; Zhang, 2019), particularly downstream of the Nile (Mediterranean Sea), the Danube (Black Sea) and the fluvial system of the Baltic Sea. Damming is a critical issue for major rivers of the tropical zone (Amazon, Congo, Changjiang, Huanghe, Ganges, Brahmaputra, etc.), which carry 74 % of the global exorheic dSi flux (Dürr et al., 2011; Tréguer et al., 1995). Among these major rivers, the course of Amazon and Congo are, so far, not affected by a dam or, if so for the Congo river, the consequence of Congo damming for the Si cycle in the equatorial african coastal system has not been studied. The case for Changjiang (Yangtze), one of the major world players on dSi delivery to the ocean, is of particular interest. Interestingly, the Changjiang (Yangtze) river dSi concentrations decreased dramatically from 1960s to 2000 (before the building of the Three Gorges Dam, TGD). This decrease is attributed to a combination of natural and anthropogenic impacts (Wang et al., 2018a). Paradoxically, since the construction of the TGD (2006 - 2009) no evidence of additional retention of dSi by the dam has been demonstrated (Wang et al., 2018a).

Over the 21st century, the influence of climate change, and other anthropogenic modifications, will have variable impacts on the regional and global biogeochemical cycling of Si. The input

Supprimé: «

of dSi will likely increase in specific regions (e.g. Arctic Ocean), whilst inputs to the global ocean might decrease. Global warming will increase stratification of the surface ocean, leading to a decrease of dSi inputs from the deep sea, although this is unlikely to influence the Southern Ocean (see Section 5.3.3). Model-based predictions suggest a global decrease in diatom production, with a subsequent decrease in export production and Si burial rate. Clearly, new observations are needed to validate model predictions.

## 6. Conclusions/recommendations

The main question that still needs to be addressed is whether the contemporary marine Si cycle is at steady state, which requires the uncertainty in total inputs and outputs to be minimized.

For the input fluxes, more effort is required to quantify groundwater input fluxes, particularly using geochemical techniques to identify the recycled marine flux from other processes that generate a net input of dSi to the ocean. In light of laboratory experiments by Fabre et al. (2019) demonstrating low temperature dissolution of quartz in clastic sand beaches, collective multinational effort should examine whether sandy beaches are major global dSi sources to the ocean. Studies addressing uncertainties at the regional scale are critically needed. Further, better constraints on hydrothermal inputs (for the North-East Pacific specific case), aeolian input and subsequent dissolution of minerals both in the coastal and in open ocean zones, and inputs from ice melt in polar regions are required.

For the output fluxes, it is clear that the alkaline digestion of biogenic silica (DeMaster, 1981; Mortlock & Froelich, 1989; Müller and Schneider, 1993), one of the commonly used methods for bSi determination in sediments, is not always effective at digesting all the bSi present in sediments. This is especially true for highly silicified diatom frustules, radiolarian tests, or sponge spicules (Maldonado et al., 2019; Pickering et al. 2020). Quantitative determination of bSi is particularly difficult for lithogenic or silicate-rich sediments (e.g. estuarine and coastal zones), for example those of the Chinese seas. An analytical effort for the quantitative determination of bSi from a variety of sediment sources and the organization of an international comparative analytical exercise are of high priority for future research. It is also clear that reverse weathering processes are important not only in estuarine or coastal environments, but also in distal coastal zones, slope, and open ocean regions of the global ocean (Baronas et al., 2017; Ehlert et al., 2016a; Geilert et al., 2020; Michalopoulos & Aller, 2014; Pickering et al., 2020; Chong et al., 2016). Careful use of geochemical tools (e.g.  $^{32}\text{Si}$ , Ge/Si,  $\delta^{30}\text{Si}$ ; Pickering et al., 2020; Geilert et al., 2020; Ehlert et al., 2016; Ng et al., 2019; Cassarino et al., in press) to

722 trace partitioning of bSi between opal and authigenic clay phases may further elucidate the  
723 magnitude of this sink, particularly in understudied areas of the ocean.  
724 This review highlights the significant progress that has been made in the past decade toward  
725 improving our quantitative and qualitative understanding of the sources, sinks and internal  
726 fluxes of the marine Si cycle. Filling the knowledge gaps identified in this review is also  
727 essential if we are to anticipate changes in the Si cycle, and their ecological and biogeochemical  
728 impacts, in the future ocean.

729

730 *Data availability:* All data used in this review article are available in the referenced articles.  
731 Data of biogenic pelagic production are shown in Supplement (Annex 1).

732

733 *Supplement:* The supplement related to this article is available on line at...XXX

734

735 *Author contributions.* PJT & JNS defined the manuscript content and wrote the paper. MAC,  
736 CE, JH, SR, OR & PT wrote the inputs section. JS, CE, SR, & MM wrote the outputs section.  
737 MB, TD, SD, AL, & PT wrote the pelagic production section. MLA & MM wrote the sponge  
738 subsections. SML, LR, & PT wrote the discussion section. Every author re-read and approved  
739 the review article.

740

741 *Competing interests.* The authors declare that they have no conflict of interest.

742

743 *Acknowledgements.* The idea for this manuscript was conceived during a conference of the  
744 SILICAMICS Network, held in June 2018 at the University of Victoria (Canada). This work  
745 was supported by the French National Research Agency (18-CEO1-0011-01), and by the  
746 Spanish Ministry of Science, Innovation and Universities (PID2019-108627RB-I00). Thanks  
747 are due to Sébastien Hervé (LEMAR-IUEM, Plouzané) for his art work.

748

## 749 **References**

750 Aller, R. C., Blair, N.E., Xia, Q., & Rude, P.D.: Remineralization rates, recycling, and storage  
751 of carbon in Amazon shelf sediments, Cont. Shelf Res., 16, 753–786, 1996.  
752 Aller, R.C.: Sedimentary diagenesis, depositional environments, and benthic fluxes, in: Treatise  
753 on Geochemistry: Second edition, edited by: Holland, H.D., & Turekian, K.K.,

Elsevier, Oxford, 8, 293–334, 2014.

Aller, R.C., Blair, N.E., & Brunskill, G.J.: Early diagenetic cycling, incineration, and burial of sedimentary organic carbon in the central Gulf of Papua (Papua New Guinea), *J. Geophys. Res. Earth Surf.*, 113, 1-22, 2008.

Anschutz, P., Smith, T., Mouret, A., Deborde, J., Bujan, S., Poirier, D., Lecroart, P.: Tidal sands as biogeochemical reactors, *Estuar. Coast. Shelf Sci.*, 84, 84–90, 2009.

Bevington, P.R., Robinson, D.K., 2003. *Data Reduction and Error Analysis for the Physical Sciences*, third ed., McGrawHill, NewYork, 2003.

Arsouze, T., Dutay, J. C., Lacan, F., & Jeandel, C.: Reconstructing the Nd oceanic cycle using a coupled dynamical - biogeochemical model. *Biogeosciences*, 6, 2829-2846, 2009.

Aumont, O., Ethé, C., Tagliabue, A., Bopp, L., & Gehlen, M.: PISCES-v2, an ocean biogeochemical model for carbon and ecosystem studies, *Geosci. Model Dev.*, 8, 2465–2513, 2015.

Aumont, O., Maier-Reimer, E., Blain, S., & Monfray, P.: An ecosystem model of the global ocean including Fe, Si, P co-limitations, *Glob. Biogeochem. Cycles*, 17, 1060, doi:10.1029/2001GB001745, 2003.

Baines, S.B., Twining, B.S., Brzezinski, M.A., Krause, J.W., Vogt, S., Assael, D., McDaniel, H.: Significant silicon accumulation by marine picocyanobacteria, *Nat. Geosci.*, 5, 886–891, 2012.

Baronas, J.J., Hammond, D.E., McManus, J., Wheat, C.G., & Siebert, C.A.: Global Ge isotope budget, *Geochim. Cosmochim. Acta*, 203, 265-83, 2017.

Beck, A. J., Charette, M. A., Cochran, J. K., Gonneea, M. E., Peucker-Ehrenbrink, B.: Dissolved strontium in the subterranean estuary - Implications for the marine strontium isotope budget. *Geochim. Cosmochim. Acta*. 117, 33–52, 2013.

Behrenfeld, M. J., & Falkowski, P. G.: Photosynthetic rates derived from satellite-based chlorophyll concentration, *Limnol. Oceanogr.*, 42, 1-20, 1997.

Bernard, C.Y., Dürr, H.H., Heinze, C., Segsneider, J., & Maier-Reimer, E.: Contribution of riverine nutrients to the silicon biogeochemistry of the global ocean – a model study, *Biogeosciences*, 8, 551–564, 2011.

Bernard, C.Y., Laruelle, G.G., Slomp, C.P., & Heinze, C.: Impact of changes in river fluxes on silica on the global marine silicon cycle: a model comparison, *Biogeosciences*, 7, 4441-453, 2010.

Berner, R.A., Lasaga, A.C., Garrels, R.M.: The carbonate-silicate geochemical cycle and its effect on atmospheric carbon dioxide over the past 100 millions years. *Am. J. Sci.*, 283,



789 Bopp, L., Resplandy, L., Orr, J.C., Doney, S.C., Dunne, J.P., Gehlen, M., Halloran, P., Heinze,  
790 C., Ilyina, S  f  rian, R., Tjiputra, J., M. Vichi, M.: Multiple stressors of ocean  
791 ecosystems in the 21st century: Projections with CMIP5 models, *Biogeosciences*, 10,  
792 6225-6245, 2013.

Boyd, P.W., Cornwall, C.E., Davison, A., Doney, S.C., Fourquez, M., Hurd, C.L., Lima, I.D.,  
McMinn, A.: Biological responses to environmental heterogeneity under future ocean  
conditions, *Glob. Change Biol.*, 22, 2633-2650, 2016.

Brzezinski, M.A., Baines, S.B., Balch, W.M., Beucher, C.P., Chai, F., Dugdale, R.C., Krause, J.W., Landry, M.R., Marchi, A., Measures, C.I., Nelson, D.M., Parker, A.E., Poulton, A.J., Selph, K.E., Strutton, P.G., Taylor, A.G., Twining, B.S.: Twining, Co-limitation of diatoms by iron and silicic acid in the equatorial Pacific, Deep Sea Res. Part II Top. Stud. Oceanogr., 58, 493–511, 2011.

Brzezinski, M.A. & Nelson, D.M.: Chronic substrate limitation of silicic acid uptake rates in the western Sargasso Sea. *Deep Sea Res. Part II Top. Stud. Oceanogr.*, 43, 437–453, 1996.

Brzezinski, M.A., Villareal, T.A., & Lipschultz, F.: Silica production and the contribution of diatoms to new and primary production in the central North Pacific, *Mar. Ecol. Prog. Ser.*, 167, 89–104, 1998.

25

822 Cassarino, L., Hendry, K. R., Henley, S. F., MacDonald, E., Arndt, S., Sales de Freitas, F., Pike,  
823 J., Firing, Y.L. : Sedimentary nutrient supply in productive hotspots off the West  
824 Antarctic Peninsula revealed by silicon isotopes. *Glob. Biogeochem. Cycles*, in press.

825 Charette M.A., Kipp, L.E., Jensen, L.T., Dabrowski, J.S., Whitmore, L.M., Fitzsimmons, J.N.,  
826 Williford, T., Ulfsbo, A., Jones, E., Bundy, R. : The Transpolar Drift as a Source of  
827 Riverine and Shelf-Derived Trace Elements to the Central Arctic Ocean, *J. G. R.*  
828 *Oceans*, 125, [e2019JC015920], 2020, DOI:10.1029/2019jc015920

829 Chase, Z., Kohfeld, K.E., Matsumoto, K.: Controls on biogenic silica burial in the Southern  
830 Ocean, *Glob. Biogeochem. Cycles*, 29, 1599–1616, 2015.

831 Cho, H.-M., Kim, G., Kwon, E.Y., Moosdorf, N., Garcia-Orellana, J., Santos, I.R.: Radium  
832 tracing nutrient inputs through submarine groundwater discharge in the global ocean,  
833 *Sci. Rep.*, 8, 2439, 2018.

834 Chong, L.S., Berelson, W., Hammond, D.E., Fleisher, M.Q., Anderson, R.F., Rollins, N.E.,  
835 Lund, S.: Biogenic sedimentation and geochemical properties of deep-sea sediments of  
836 the Demerara slope/abyssal Plain: Influence of the Amazon River Plume, *Mar. Geol.*,  
837 379, 124-139, 2016.

838 Chou, C. & Neelin, J.D.: Mechanisms of global warming impacts on regional tropical  
839 precipitations, *J. Clim.*, 17, 2688-2701, 2004.

840 Chou, C., Neelin, J.D., Chen, C.-A., & Tu, J.-Y.: Evaluating the “rich-get-richer” mechanism  
841 in tropical precipitation change under global warming, *J. Clim.*, 22, 1982-2005, 2008.

842 Conley, D.J.: An interlaboratory comparison for the measurement of biogenic silica in  
843 sediments, *Mar. Chem.*, 63, 39-48, 1988.

844 Conley, D.J, Likens, G.E., Buso, D.C., Saccone, L., Bailey, S.W., Johnson, C.E.: Deforestation  
845 causes increased dissolved silicate losses in the Hubbard Brook Experimental Forest,  
846 *Glob. Change Biol.*, 14, 2458-2554, 2008.

847 Conley, D.J., Frings, P.J., Fontorbe, G., Clymans, W., Stadmark, J., Hendry, K.R., Marron,  
848 A.O., De La Rocha, C.L.: Biosilicification drives a decline of dissolved Si in the oceans  
849 through geologic time, *Front. Mar. Sci.*, 4, 397, 2017.

850 Conley, D.J., Schelske, C.L., & Stoermer, E.F.: Modification of the biogeochemical of silica  
851 with eutrophication, *Mar. Ecol. Progr. Ser.*, 101, 179-192, 1993.

852 De Souza, G.F., Slater, R.D., Dunne, J.P., & Sarmiento, J.L.: Deconvolving the controls on the  
853 deep ocean’s silicon stable isotope distribution, *Earth Planet. Sci. Lett.*, 398, 66–76,  
854 2014.

855 DeMaster, D.J.: The accumulation and cycling of biogenic silica in the Southern Ocean:

revisiting the marine silica budget, *Deep Sea Res. Part II Top. Stud. Oceanogr.*, 49, 3155–3167, 2002.

DeMaster, D.J.: The supply and accumulation of silica in the marine environment, *Geochim. Cosmochim. Acta*, 45, 1715-1732, 1981.

Derry, L.A., Kurtz, A.C., Ziegler, K., & Chadwick, O.A.: Biological control of terrestrial silica cycling and export fluxes to watershed, *Nature*, 433, 728-731, 2005.

Ding, S., Chen, P., Liu, S.M., Zhang, G., Zhang, J., Dan, S.F.: Nutrient dynamics in the Changjiang and retention effect in the Three Gorges Reservoir. *J. Hydrol.*, 574, 96–109, 2019.

Dunne, J.P., Sarmiento, J.L., & Gnanadesikan, A.: A synthesis of global particle export from the surface ocean and cycling through the ocean interior and on the seafloor, *Glob. Biogeochem. Cycles*, 21, GB4006, 2007.

Duprat, L.P.A.M., Bigg, G.R., Winton, D.J.: Enhanced Southern Ocean marine productivity due to fertilization by giant icebergs, *Nature Geosci.*, 9, 219-221, 2016.

Dürr H.H., Meybeck, M., Hartmann, J., Laruelle, G.G., & Roubeix, V.: Global spatial distribution of natural riverine silica inputs to the coastal zone, *Biogeosciences*, 8, 597–620, 2011.

Dutkiewicz, S., Hickman, E., Jahn, O., Henson, S., Beaulieu, B. & Monier, E.: Ocean colour signature of climate change, *Nat. Comm.*, 10, 019, 2019.

Dutkiewicz, S., Hickman, A.E., Jahn, O., Gregg, W.W., Mouw, C.B., & Follows, M.J.: Capturing optically important constituents and properties in a marine biogeochemical and ecosystem model, *Biogeosciences*, 12, 4447–4481, 2015.

Edmond, J.M., Measures, C., Mangum, B., Grant, B., F. R. Sclater, F. R., Collier, R., Hudson, A., Gordon, L. I., Corliss, J. B.: On the formation of metal-rich deposits at ridge crests, *Earth. Planet. Sci. Lett.*, 46, 19-30, 1979.

Ehlert, C., Doeringa, K. Wallmanna, K., Scholza, F., Sommera, S., Grasse, P., Geilert, S., Frank, M.: Stable silicon isotope signatures of marine pore waters – Biogenic opal dissolution versus authigenic clay mineral formation, *Geochim. Cosmochim. Acta*, 191, 102–117, 2016a.

Ehlert, C., Reckhardt, A., Greskowiak, J., Liguori, B.T.P., Böning, P., Paffratha, R., Brumsack, H.-J., Pahnke, K.: Transformation of silicon in a sandy beach ecosystem: insights from stable silicon isotopes from fresh and saline groundwaters, *Chem. Geol.*, 440, 207–218, 2016b.

Elderfield, H. & Schultz, A.: Mid-ocean ridge hydrothermal fluxes and the chemical

composition of the ocean, *Ann. Rev. Earth Planet. Sci.*, 24, 191-224, 1996.

Escoube, R., Rouxel, O., Edwards, K., Glazer, B. and Donard, O.: Coupled Ge/Si and Ge isotope ratios as geochemical tracers of seafloor hydrothermal systems: case studies at Loihi Seamount and East Pacific Rise 9°50'N. *Geochim. Cosmochim. Acta*, 167, 93-112, 2015.

Fabre, S., Jeandel, C., Zambardi, T., Roustan, M., & Almar, R.: An overlooked silica source of the modern oceans: are sandy beaches the key? *Front. Earth Sci.*, 7, 231, 2019.

Fillinger, L., Janussen, D., Lundälv, T., Richter, C.: Rapid glass sponge expansion after climate-induced Antarctic ice shelf collapse, *Curr. Biol.*, 23, 1330-1334, 2013.

Finney, B.P., Lyle, M.W., Heath, G.R.: Sedimentation at MANOP Site H (eastern equatorial Pacific) over the past 400,000 years: Climatically induced redox variations and their effects on transition metal cycling, *Paleoceanogr.*, 1988. <https://doi.org/10.1029/PA003i002p00169>

Franck, V.M., Brzezinski, M.A., Coale, K.H., & Nelson, D.M.: Iron and silicic acid concentrations regulate Si uptake north and south of the Polar Frontal Zone in the Pacific Sector of the Southern Ocean, *Deep. Res. Part II Top. Stud. Oceanogr.*, 47, 3315–3338, 2000.

Frings, P.: Revisiting the dissolution of biogenic Si in marine sediments: a key term in the ocean Si budget, *Acta Geochim.*, 36, 429–432, 2017.

Frings, P.J., Clymans, W., Fontorbe, G., De La Rocha, C.L., & Conley, D.J.: The continental Si cycle and its impact on the ocean Si isotope budget. *Chem. Geol.*, 425, 12–36, 2016.

Galy, V.C., France-Lanord, C., Beysac, O., Faure, P., Kudrass, H., & Pahol, F.: Efficient organic carbon burial in the Bengal fan sustained by the Himalayan erosional system, *Nature*, 450, 407-410, 2007.

Garcia, H. E., Locarnini, R.A., Boyer, T.P., Antonov, J.I., Baranova, O.K., Zweng, M.M., Reagan, J.R., & Johnson, D.R.: Dissolved Inorganic Nutrients (phosphate, nitrate, silicate), in: *World Ocean Atlas 2013*, edited by Levitus, Mishonov A., NOAA Atlas NESDIS 76, 25 pp., 2014.

Garcia, H.E., Weathers, K.W., Paver, C.R., Smolyar, I., Boyer, T.P., Locarnini, M.M., Zweng, M.M., Mishonov, A.V., Baranova, O.K., Seidov, D., Reagan, J.R.: Dissolved Inorganic Nutrients (phosphate, nitrate, silicate), in: *World Ocean Atlas 2018*, edited by Levitus, Mishonov A., NOAA Atlas NESDIS 84, 35 pp., 2019, [https://data.nodc.noaa.gov/woa/WOA18/DOC/woa18\\_vol4.pdf](https://data.nodc.noaa.gov/woa/WOA18/DOC/woa18_vol4.pdf)

923 Geibert, W., Rutgers van der Loeff, M.M., Usbeck, R., Gersonde, R., Kuhn, G., Seeberg-  
 924 Elverfeldt, J.: Quantifying the opal belt in the Atlantic and southeast Pacific sector of  
 925 the Southern Ocean by means of  $^{230}\text{Th}$  normalization, *Glob. Biogeochem. Cycles*, 19,  
 926 GB4001, 2005.

927 Geilert, S., Grasse, P., Wallmann, K., Liebetrau, V., Menzies, C.D.: Serpentine alteration as  
 928 source of high dissolved silicon and elevated  $\delta^{30}\text{Si}$  values to the marine Si cycle, *Nature*  
 929 *comm.*, 2020. <https://doi.org/10.1038/s41467-020-18804-y>

930 Georg, R.B., West, A.J., Basu, A.R., & Halliday, A.N.: Silicon fluxes and isotope composition  
 931 of direct groundwater discharge into the Bay of Bengal and the effect on the global  
 932 ocean silicon isotope budget, *Earth Plant. Sci. Lett.*, 203, 67-74, 2009.

933 Gnanadesikan, A., & Toggweiler, J.R.: Constraints placed by silicon cycling on vertical  
 934 exchange in general circulation models. *Geophys. Res. Lett.*, 26, 1865–1868, 1999.

935 Graly, J.A., Humphrey, N.F., Landowski, C.M., Tarper, J.T.: Chemical weathering under the  
 936 Greenland Ice Sheet, *Geology*, 42, 551-554, 2014.

937 Hatton, J.E., Hendry, K.R., Hawkings, J.R., Wadham, J.L., Kohler, T.J., Stibal, M., Beaton,  
 938 A.D., Bagshaw, E.A., Telling, J.: Investigation of subglacial weathering under the  
 939 Greenland Ice Sheet using silicon isotopes, *Geochim. Cosmochim. Acta*, 247, 191–206,  
 940 2019.

941 Hatton, J.E., Hendry, K.R., Hirst, C., Opfergelt, S., Henkel, S., Silva-Busso, A., Welch, S.A.,  
 942 Wadham, J.L., Lyons, W.B., Bagsaw, E., Staubwasser, M., McKnight, D.: Silicon  
 943 Isotopic Composition of Dry and Wet-Based Glaciers in Antarctica, *Frontiers Earth Sci.*,  
 944 8 (286), 2020. doi: 10.3389/feart.2020.00286

945 Hautala, S., Hammond, D.E.: Abyssal pathways and the double maximum in the northeast  
 946 Pacific basin. *Geophys. Res. Lett.*, 2020. 10.1029/2020GL089010

947 Hawkings, J. R., Hatton, J.E., Hendry, K. R., de Souza, G. F., Wadham, J. L., Ivanovic, R.,  
 948 Kohler, T. J., Stibal, M., Beaton, A., Lamarche-Gagnon, G., Tedstone, A., Hain, M. P.,  
 949 Bagshaw, E., Pike, J., Tranter, M.: The silicon cycle impacted by past ice sheets, *Nat.*  
 950 *Commun.*, 9, 3210, 2018.

951 Hawkings, J.R., Wadham, J.L., Benning, L.G., Hendry, K.R., Tranter, M., Tedstone, A.,  
 952 Nienow, P. & Raiswell, R. : Ice sheets as a missing source of silica to the polar oceans.  
 953 *Nat. Commun.*, 8, 14198, 2017.

954 Hawkings, J. R., Skidmore, M. L., Wadham, J. L., Priscu, J. C., Morton, P. L., Hatton, J. E.,  
 955 Gardner, C. B., Kohler, T. J., Stibal, M., Bagshaw, E. A., Steigmeyer, A., Barker, J.,  
 956 Dore, J. E., Lyons, W. B., Tranter, M., Spencer, R. G. M. (2020) Enhanced trace element

957 mobilization by the Earth's ice sheets, *Proceedings of the National Academy of Science*,  
958 2020. DOI: 10.1073/pnas.2014378117.

959 Hayes, C.T., Costa, K.M., Anderson, R.F., Calvo, E., Chase Z., Demina L.L., Dutay, J.-C.,  
960 German, C.R., Heimbürger-Boavida, L.-E., Jaccard, S.L., Jacob, A., Kohfeld, K.E.,  
961 Kravchishina, M.D., Lippold, J., Mekik, F., Missiaen, L., Pavia, F.J., Paytan, A.,  
962 Pamies, Pedrosa-Pamies, R., Petrova, M.V., Rahman, S., Robinson L.F., Roy-Barman,  
963 M., Sanchez-Vidal, A., Shiller, A., Tagliabue, A., Tessin, A.C., van Hulten, M., Zhang  
964 J.: Global ocean sediment composition and burial flux in the deep sea, *Glob. Biogeo.*  
965 *Cy.* (under review).

966 Heinze, C., Hupe, A., Maier-Reimer, E., Dittert, N., and Ragueneau, O.: Sensitivity of the  
967 marine biospheric Si cycle for biogeochemical parameter variations, *Global*  
968 *Biogeochem. Cy.*, 17, 1086, doi:10.1029/2002GB001943, 2003.

969 Hendry, K.R., Huvenne, V.A.I., Robinson, L.F., Annett, A., Badger, M., Jacobel, A.W, Ng,  
970 H.C., Opher, J., Pickering, R.A., Taylor, M.L., Bates, S.L., Cooper, Z., Cusham, G.G.,  
971 Goodwin, C., Hoy, S., Rowland, G., Samperiz, A., Williams, J.A., Woodward, M.S. :  
972 The biogeochemical impact of glacial meltwater from Southwest Greenland, *Progress*  
973 *in Oceanogr.*, 2019. doi: <https://doi.org/10.1016/j.pocean.2019.102126>

974 Henley, S.F., Schofield, O.M., Hendry, K.R., Schloss, I.R., Steinberg, D.K, Moffath, C., Peck,  
975 L.S., Costa, D.P., Bakker, D.C.E., Hughes, C., Rozema, P.D., Ducklow, H.W., Abele,  
976 D., Stefels, J., Van Leeuwe, M.A., Brussaard, C.P.D., Buma, A.G.J., Kohu, J., Sahade,  
977 R., Friedlaender, A.S., Stammerjohn, S.E., Venables, H.J., Meredith, M.P.: Variability  
978 and change in the west Antarctic Peninsula marine system: Research priorities and  
979 opportunities, *Progr. Oceanogr.*, 173, 208\_237, 2019.

980 Henson, S. A., Sarmiento, J. L., Dunne, J. P., Bopp, L., Lima, I., Doney, S. C., John, J.,  
981 Beaulieu, C.: Detection of anthropogenic climate change in satellite records of ocean  
982 chlorophyll and productivity, *Biogeosciences*, 7, 621–640, 2010.

983 Herraiz-Borreguero, L., Lannuzel, D., van der Merwe, P., Treverrow, A., Pedro, J.B.: Large  
984 flux of iron from the Amery Ice Shelf marine ice to Prydz Bay, East Antarctica, *J.*  
985 *Geophys. Res.: Oceans*, 121, 6009-6020, 2016.

986 Hinder, S. L., Hays, G. C., Edwards, M., Roberts, E. C., Walne, A. W., Gravenor, M. B.:  
987 Changes in marine dinoflagellate and diatom abundance under climate change, *Nat.*  
988 *Clim. Chang.*, 2, 271–275, 2012.

989 Hirst, C., Opfergelt, S., Gaspard, F., Hendry, K.R., Hatton, J.E., Welch, S., McKnight, D.M.,  
990 Lyons, W.B. : Silicon Isotopes Reveal a Non-glacial Source of Silicon to Crescent

991 Stream, McMurdo Dry Valleys, Antarctica, *Frontiers Earth Sci.*, 8 (229), 2020. doi:  
 992 10.3389/feart.2020.00229

993 Holzer, M., Primeau, F.W., DeVries, T., & Matear, R.: The Southern Ocean silicon trap: Data-  
 994 constrained estimates of regenerated silicic acid, trapping efficiencies, and global  
 995 transport paths, *J. Geophys. Res. Ocean*, 119, 313–33, 2014.

996 Hou Y., Hammond, D. E.; Berelson, W.M.; Kemnitz, N.; Adkins, J.F.; Lunstrum, A.: Spatial  
 997 patterns of benthic silica flux in the North Pacific reflect upper ocean production, *Deep-  
 998 Sea Research Part I*, 148, 25–33, 2019.

999 Humborg C., Pastuszak, M., Aigars, J., H. Siegmund, H., Mörrh, C.-M., Ittekkot, V.: Decreased  
 1000 silica land-sea fluxes trough damming in the Baltic Sea catchment –significance of  
 1001 particle trapping and hydrological alteration, *Biogeochemistry* 77, 265-281, 2006.

1002 Hutchins, D.A. & Boyd, P.W.: Marine phytoplankton and the changing ocean iron cycle. *Nat.*  
 1003 *Clim. Change*, 6, 1072-1076, 2016.

1004 IPCC 2018 [https://www.ipcc.ch/2018/10/08/summary-for-policymakers-of-ipcc-special-](https://www.ipcc.ch/2018/10/08/summary-for-policymakers-of-ipcc-special-report-on-global-warming-of-1-5c-approved-by-governments/)  
 1005 [report-on-global-warming-of-1-5c-approved-by-governments/](https://www.ipcc.ch/2018/10/08/summary-for-policymakers-of-ipcc-special-report-on-global-warming-of-1-5c-approved-by-governments/)

1006 Ittekkot, V, Humborg C, Schäfer P.: Hydrological alternations and marine biogeochemistry: a  
 1007 silicate issue? *BioScience*, 50, 776–82, 2000.

1008 Ittekkot, V., Unger, D., Humborg, C., Tac An, N. T. (Eds): *The Silicon Cycle: Human  
 1009 Perturbations and Impacts on Aquatic Systems*, Comm. Probl. Environ. (SCOPE) Ser.  
 1010 Vol. 66. Washington, DC: Island. 296 pp, 2006.

1011 Jeandel, C.: Overview of the mechanisms that could explain the ‘Boundary Exchange’ at the  
 1012 land–ocean contact, *Philos. Trans. R. Soc. A Math. Phys. Eng. Sci.*, 374, 20150287,  
 1013 2016.

1014 Jeandel, C., Peucker-Ehrenbrink B., Jones, M.T., Pearce, C.R., Oelkers, E.H., Godderis, Y.,  
 1015 Lacan, F., Aumont, O., Arsouze, T. : Ocean margins : the missing term for oceanic  
 1016 element budgets ? *Eos Trans. AGU*, 92, 217, 2011.

1017 Jeandel, C. & Oelkers, E.H.: The influence of terrigenous particulate material dissolution on  
 1018 ocean chemistry and global elements cycles, *Chem. Geol.*, 395, 50-56, 2015.

1019 Jin, X., Gruber, N. Dunne, J.P., Sarmiento, J.L., & Armstrong R.A.: Diagnosing the  
 1020 contribution of phytoplankton functional groups to the production and export of  
 1021 particulate organic carbon, CaCO<sub>3</sub>, and opal from global nutrient and alkalinity  
 1022 distributions, *Glob. Biogeochem. Cycles*, 20, GB2015, 2006.

1023 Jochum, K. P., Schuessler, J.A., Wang, X.-H., Stoll, B., Weis, U., Müller, W.E.G., Haug, G.H.,

1024 Andreae, M.O., Froelich, P.N.: Whole-ocean changes in silica and Ge/Si ratios during  
 1025 the last deglacial deduced from long-lived giant glass sponges, *Geophys. Res. Lett.*, 44,  
 1026 555-564, 2017.

1027 Johnson, R., Strutton, P.G., Wright, S.W., McMinn, A., Meiner, K.M.: Three improved satellite  
 1028 chlorophyll algorithms for the Southern Ocean, *J. Geophys. Res. Oceans*, 118, 3694–  
 1029 3703, 2013. doi:10.1002/jgrc.20270

1030 Johnson, H.P., Hautala, S.L., Bjorklund, T.A., Zarnetske, M.R.: Quantifying the North Pacific  
 1031 silica plume, *Geoch. Geophys. Geosyst.*, 2006. <https://doi.org/10.1029/2005GC001065>

1032 Jones, M., Pearce, C.R., Oelkers, E.H.: An experimental study of the interaction of basaltic  
 1033 riverine particulate material and seawater *Geochim. Cosmochim. Acta*, 77, 108-120,  
 1034 2012.

1035 Krause, J.W., Mark A. Brzezinski, M.A., Baines, S.B., Collier, J.L., Twining, B.S., Ohnemus,  
 1036 D.C.: Picoplankton contribution to biogenic silica stocks and production rates in the  
 1037 Sargasso Sea, *Glob. Biogeochem. Cycles*, 31, 762–774, 2017.

1038 Krause, J.W., Brzezinski, M.A., Villareal, T.A., & Wilson, W.: Increased kinetic efficiency for  
 1039 silicic acid uptake as a driver of summer diatom blooms in the North Pacific subtropical  
 1040 gyre, *Limnol. Oceanogr.*, 57, 1084–1098, 2012.

1041 Laruelle, G.G., Roubex, V., Sferratore, A., Brodherr, B., Ciuffa, D., Conley, D.J., Dürr, H.H.,  
 1042 Garnier, J., Lancelot, Le Thi Phuong, Q., Meunier, J.-D., Meybeck, M.,  
 1043 Michalopoulos, P., Moriceau, B., Ní Longphuirt, S., Loucaides, S., Papush, L., Presti,  
 1044 M., Ragueneau, O., Regnier, P.A.G., Saccone, L., Slomp, C.P., , Spiteri, C., Van  
 1045 Cappelle, P. : Anthropogenic perturbations of the silicon cycle at the global scale: key  
 1046 role of the land-ocean transition, *Glob. Biogeochem. Cycles*, 23, GB4031, 1-17, 2009.

1047 Laufkötter, C., Vogt, M., Gruber, Aita-Noguchi, M., Aumont, O., Bopp, L., Buitenhuis, E.,  
 1048 Doney, S.C., Dunne, J., Hashioka, T., Hauck, J., Hirata, T., John, J., Le Quéré, C., Lima,  
 1049 I.D., NakanoH., Seferian, R., Totterdell, I., Vichi, M., Völker, C.: Divers and  
 1050 uncertainties of future global marine primary production in marine ecosystem models,  
 1051 *Biogeosciences*, 12, 6955–6984, 2015.

1052 Leinen, M., Cwienk, D., Heath, G.R., Biscaye, P.E., Kolla, V., Thiede, J., Dauphin, J.P.:  
 1053 Distribution of biogenic silica and quartz in recent deep-sea sediments, *Geology*, 14,  
 1054 199–203, 1986

1055 Li, D., Dong, M., Liu, S., Chen, H., & Yao, Q.: Distribution and budget of biogenic silica in  
 1056 the Yangtze Estuary and its adjacent sea, *Sci. Total Environ.*, 669, 590–599 (2019).

1057 Li, L, Barry, D.A., Stagnitti, F., & Parlange, J.Y.: Submarine groundwater discharge and



1058 associated chemical input to a coastal sea, *Water Resources Res.*, 35, 3253-3259, 1999.

1059 Lippold, J., Luo, Y., Francois, R., Allen, S.E., Gherardi, J., Pichat, S., Hickey, B., Schulz, H.:  
1060 Strength and geometry of the glacial Atlantic Meridional Overturning Circulation,  
1061 *Nature Geosci.*, 5, 813–816, 2012.

1062 Liu, J., Du, J., & Yi, L.: Ra tracer-based study of submarine groundwater discharge and  
1063 associated nutrient fluxes into the Bohai Sea, China: A highly human-affected marginal  
1064 sea, *J. Geophys. Res. Ocean*, 122, 8646–8660, 2017a.

1065 Liu, J., Su, N., Wang, X., & Du, J.: Submarine groundwater discharge and associated nutrient  
1066 fluxes into the Southern Yellow Sea: A case study for semi-enclosed and oligotrophic  
1067 seas-implication for green tide bloom, *J. Geophys. Res. Ocean*, 122, 139–152, 2017b.

1068 Liu, J., Zang, J., Bouwman, L., Liu, S., Yu, Z., Ran, X.: Distribution and budget of dissolved  
1069 and biogenic silica in the Bohai Sea and Yellow Sea, *Biogeochemistry*, 130, 85–101  
1070 2016.

1071 Liu, S.M., L.W., Zhang, G.L., Liu, Z., Yu, Z., & Ren, J.L.: Impacts of human activities on  
1072 nutrient transports in the Huanghe (Yellow River) Estuary, *J. Hydrol.*, 430-431, 103-  
1073 110, 2012.

1074 Liu, S.M., Zhang, J., & Li, R.X.: Ecological significance of biogenic silica in the East China  
1075 Sea, *Mar. Ecol. Prog. Ser.*, 290, 15–26, 2005.

1076 Llopis Monferrer, N., Boltovskoy, D., Tréguer, P., Méndez Sandin, M., Not, F., Leynaert, A.:  
1077 Estimating biogenic silica production of Rhizaria in the global ocean, *Glob.*  
1078 *Biogeochem. Cycles*, 34, e2019GB006286, 2020.

1079 Longhurst, A., S. Sathyendranath, T. Platt, Caverhill, C.: An estimate of global primary  
1080 production in the ocean from satellite radiometer data, *J. Plankton Res.*, 17, 1245–1271,  
1081 1995.

1082 Longhurst, A.R. (Ed.) : *Ecological Geography of the Sea*, Academic Press, London, ed. 2nd,  
1083 2007.

1084 Luijendijk, A., Hagenaars, G., Roshanka, R., Baart, F., Donchyts, G., Aarninkhof, S.: The state  
1085 of the world's beaches, *Sci. Rep.*, 8, 6641, 2018.

1086 Maldonado M., Navarro L., Grasa A., Gonzalez A., Vaquerizo I.: Silicon uptake by sponges: a  
1087 twist to understanding nutrient cycling on continental margins, *Sci. Rep.*, 1, 30, 2011.

1088 Maldonado, M., Ribes, M. & van Duyl, F. C.: Nutrient fluxes through sponges, *Adv. Mar.*  
1089 *Biol.*, 62, 113–182, 2012.

1090 Maldonado, M., López-Acosta, M., Beazley, L., Kenchington, E., Koutsouveli, V., Riesgo, A.:  
1091 Cooperation between passive and active silicon transporters clarifies the ecophysiology

and evolution of biosilicification in sponges. *Sci. Advances*, 6, 2020.

Maldonado, M., López-Acosta, M., Sitjà, C., García-Puig, M., Galobart, C., Ercilla, G., Leynaert, A.: Sponge skeletons as an important sink of silicon in the global oceans, *Nat. Geosci.* 12, 815–822, 2019.

Matsumoto, K., Tokos, K., Huston, A., & Joy-Warren, H.: MESMO 2: a mechanistic marine silica cycle and coupling to a simple terrestrial scheme, *Geosci. Model Dev.* 6, 477–494, 2013.

Meire, L., Meire, P., Struyf, E., Krawczyk, D.W., Arendt, K.E., Yde, J.C., Pedersen, T.J., Hopwood, M.J., Rysgaard, S., Meysman, F.J.R.: High export of dissolved silica from the Greenland Ice Sheet, *Geophys. Res. Lett.* 43, 9173–9182, 2016.

Meyer, J. L., Jaekel, U., Tully, B. J., Glazer, B. T., Wheat, C. G., Lin, H.-T., Hsieh, C.-C., Cowen, J. P., Hulme, S. M., Girguis, P. R., Huber, J. A.: A distinct and active bacterial community in cold oxygenated fluids circulating beneath the western flank of the Mid-Atlantic ridge, *Sci. Rep.*, 6, 22541, 2016.

Michalopoulos, P., & Aller, R. C.: Rapid Clay Mineral Formation in Amazon Delta Sediments: Reverse Weathering and Oceanic Elemental Cycles. *Science*, 270, 614–617, 1995.

Michalopoulos, P. & Aller, R.C.: Early diagenesis of biogenic silica in the Amazon delta: alteration, authigenic clay formation, and storage, *Geochim. Cosmochim. Acta*, 68, 1061–1085, 2004.

Michaud, A. B., Skidmore, M. L., Mitchell, A. C., Vick-Majors, T. J., Barbante, C., Turetta, C., VanGelder, W., Priscu, J. C.: Solute sources and geochemical processes in Subglacial Lake Whillans, West Antarctica, *Geology*, 44, 347–350, 2016.

Moriceau, B., Gehlen, M., Tréguer, P., Baines, S., Livage, J., André, L.: Editorial: Biogeochemistry and genomics of silicification and silicifiers, *Front. Mar. Sci.* 6, 57, 2019.

Morin, G.P., Vigier, N., & Verney-Carron, A.: Enhanced dissolution of basaltic glass in brackish waters: Impact on biogeochemical cycles, *Earth Planet. Sci. Lett.*, 417, 1–8, 2015.

Mortlock, R.A., Froelich, P.N.: A simple method for the rapid determination of biogenic opal in pelagic marine sediments, *Deep Sea Res. Part A. Oceanogr. Res. Papers*, 36, 1415–1426, 1989.

Mottl, M.J.: Hydrothermal processes at seafloor spreading Centers: application of basalt-seawater experimental results. In: Rona, P.A., Boström, K., Laubier, L., Smith, K.L. (eds) *Hydrothermal Processes at Seafloor Spreading Centers*. NATO Conference Series

1126 (IV Marine Sciences), 12. Springer, Boston, MA. , 1983. [https://doi.org/10.1007/978-1-](https://doi.org/10.1007/978-1-4899-0402-7_10)  
 1127 4899-0402-7\_10  
 1128 Mottl, M.J.: Partitioning of energy and mass fluxes between mid-ocean ridge axes and flanks  
 1129 at high and low temperature, in: Energy and Mass Transfer in Marine Hydrothermal  
 1130 Systems, edited by Halbach, P.E., Tunncliffe, V., Hein, J.R., Dahlem University Press,  
 1131 pp. 271–286, 2003.  
 1132 Mottl, M. : Explanatory notes and master chemical item spreadsheet for the VentDB Data  
 1133 collections housed in the EarthChem Library, Version 1.0. Interdisciplinary Earth Data  
 1134 Alliance (IEDA), 2012. <https://doi.org/10.1594/IEDA/100207>.  
 1135 Müller, J., Schneider, R.: An automated leaching method for the determination of opal in  
 1136 sediments and particulate matter, Deep Sea Res. Part I, 40, 425-444, 1993.  
 1137 Nelson, D.M., & Goering, J.J.: Near-surface silica dissolution in the upwelling region off  
 1138 northwest Africa, Deep Sea Res., 24, 65–73, 1977.  
 1139 Nelson, D.M., Tréguer, P., Brzezinski, M.A., Leynaert, A., & Quéguiner, B.: Production and  
 1140 dissolution of biogenic silica in the ocean - Revised global estimates, comparison with  
 1141 regional data and relationship to biogenic sedimentation, Glob. Biogeochem. Cycles, 9,  
 1142 359–372, 1995.  
 1143 Ng, H.C., Cassarino, L., Pickering, R.A., Woodward, E.M.S., Hendry, K.R.: Sediment efflux  
 1144 of silicon on the Greenland margin and implications for the marine silicon cycle. Earth  
 1145 Planet Sci. Lett., 529, 115877, 2020.  
 1146 Nielsen, S. G., Rehkämper, M., Teagle, D. A. H., Butterfield, D. A., Alt, J. C. Halliday, A. N.:  
 1147 Hydrothermal fluid fluxes calculated from the isotopic mass balance of thallium in the  
 1148 ocean crust, Earth Planet. Sci. Lett., 251, 120–133, 2006.  
 1149 Oelkers, E. H., Gislason, S. R., Eiríksdóttir, E. S., Jones, M. T., Pearce, C. R., Jeandel C.: The  
 1150 role of riverine particulate material on the global cycles of the elements, Appl.  
 1151 Geochem., 26, S365–S369, 2011.  
 1152 Ohnemus, D.C., Rauschenberg, S., Krause, J.W., Brzezinski, M.A.: Silicon content of individual  
 1153 cells of *Synechococcus* from the North Atlantic Ocean, Mar. Chem., 187, 16–24, 2016.  
 1154 Opalinka, B. & Cowlings, S.A.: Modelling the movement of biogenic silica from terrestrial  
 1155 vegetation to riverine systems within the continental USA, Ecol. Model., 312, 104-113,  
 1156 2015. <https://doi.org/10.1016/j.ecolmodel.2015.05.012>  
 1157 Pasquier, B., & Holzer, M.: Inverse-model estimates of the ocean’s coupled phosphorus,  
 1158 silicon, and iron cycles, Biogeosciences, 14, 4125–4159, 2017.  
 1159 Pearce, C.R., Jones, M.T., b, Oelkers, E.H., Pradoux, C., Jeandel, C.: The effect of particulate

dissolution on the neodymium (Nd) isotope and Rare Earth Element (REE) composition of seawater, *Earth Planet. Sci. Lett.*, 369-370, 138-147, 2013.

Peng, T.-S. , Maier-Reimer, E., Broecker, W.S.: Distribution of  $^{32}\text{Si}$  in the world ocean: model compared to observation. *Glob. Biogeochem. Cycles*, 7, 464-474, 1993.

Philipps, A. Modelling riverine dissolved silica on different spatial and temporal scales using statistical and machine learning methods, Ph.D thesis, Univ. Toronto, 121 pp., 2020. <http://hdl.handle.net/1807/101210>

Pickering, R.A., Cassarino, L., Hendry, K.R., Wang, X.L., Maiti, K., Krause, J.W.: Using Stable Isotopes to Disentangle Marine Sedimentary Signals in Reactive Silicon Pools, *Geophys. Res. Lett.*, 2020. <https://doi.org/10.1029/2020GL087877>

Pondaven, P., Ragueneau, O., Tréguer, P., Hauvespre, A., Dezileau, L., Reyss, J.L.: Resolving the 'opal paradox' in the Southern Ocean, *Nature*, 405, 168-172, 2000.

Prakash Babu, C., Brumsack, J., Böttcher, M.E.: Barium as a productivity proxy in continental margin sediments: a study from the eastern Arabian Sea, *Mar. Geol.*, 184, 189-206, 2002.

Rahman, S., Aller, R.C., Cochran, & J.K.: Cosmogenic  $^{32}\text{Si}$  as a tracer of biogenic silica burial and diagenesis: Major deltaic sinks in the silica cycle, *Geophys. Res. Lett.*, 43, 7124–7132, 2016.

Rahman, S., Aller, R.C., & Cochran, J.K.: The missing silica sink: revisiting the marine sedimentary Si cycle using cosmogenic  $^{32}\text{Si}$ , *Glob. Biogeochem. Cycles*, 31, 1559–1578, 2017.

Rahman, S., Tamborski, J.J., Charette, M.A., & Cochran, J.K.: Dissolved silica in the subterranean estuary and the impact of submarine groundwater discharge on the global marine silica budget, *Mar. Chem.*, 208, 29–42, 2019.

Roshan, S., DeVries, T., Wu, J., & Chen, G.: The internal cycling of Zinc in the ocean, *Glob. Biogeochem. Cycles*, 32, 1833–1849, 2018.

Saconne, L., Conley, D.J., Koning, E., Sauer, D., Sommer, M., Kaczorek, D., Blecher, S.W., Kelly, E.F.: Assessing the extraction and quantification of amorphous silica in soils of forests and grassland ecosystems. *Eur. J. Soil Sci.*, 58, 1446-1459, 2007.

Sarmiento, J.L. & Gruber, N. : Ocean biogeochemical dynamics, Princeton University press, Princeton & Oxford, 2006.

Sarmiento, J.L., Simeon, J., Gnanadesikan, A., Gruber, N., Key, R.M., Schlitzer, R.: Deep ocean biogeochemistry of silicic acid and nitrate. *Glob. Biogeochem. Cycles*, 21, GB1S90, 2007.

1194 Siever, R.: Silica in the oceans: biological – geochemical interplay, in “Scientists in Gaia”,  
 1195 edited by : Schneider, S.H. Boston, P.J., MIT Press, 285-295, 1991.

1196 Struyf, E., Mörrh, C.-M., Humborg, C., Conley, D.J.: An enormous amorphous silica stock in  
 1197 boreal wetlands, J.G.R., 115, G04008, 2010. doi:10.1029/2010JG001324.

1198 Syvistkia, J.P.M., Peckhama, S.D., Hilbermana, R., Mulderb, T.: Predicting the terrestrial flux  
 1199 of sediment to the global ocean:a planetary perspective, Sedim. Geol., 162, 5–24, 2003.

1200 Talley, L.D., Joyce, T.M.: The double silica maximum in the North Pacific. J. Geophys. Res.,  
 1201 97, 5465-5480, 1992.

1202 Techer, I., Advocat, T., Lancelot, J., & Liotard, J.M.: Dissolution kinetics of basaltic glasses:  
 1203 Control by solution chemistry and protective effect of the alteration film, Chem. Geol.,  
 1204 176, 235–263, 2001.

1205 Tegen, I. & Kohfeld, K.E.: Atmospheric Transport of Silicon, in: The silica cycle, human  
 1206 perturbations and impacts on aquatic systems, edited by Ittekkot V. et al. anthropic, Scope  
 1207 66, 2006.

1208 Tréguer P. & Jacques, G.: Dynamics of nutrients and phytoplankton, and fluxes of carbon,  
 1209 nitrogen and silica in the Antarctic ocean, Pol. Biol., 12, 149-162, 1992.

1210 Tréguer, P., Louis Lindner, L., van Bennekom, A.J., Leynaert, A., Panouse, M., Jacques, G.:  
 1211 Production of biogenic silica in the Weddell-Scotia Seas measured with <sup>32</sup>Si, Limnol.  
 1212 Oceanogr., 36, 1217-1227, 1991.

1213 Tréguer, P., Nelson, D.M., Van Bennekom, A.J., Demaster, D.J., Leynaert, A., Quéguiner, B.:  
 1214 The balance of silica in the world ocean, Science, 268, 376-79, 1995.

1215 Tréguer, P., Bowler, C., Moriceau, B., Dutkiewicz, S., Gehlen, M., Aumont, O., Bittner, L.,  
 1216 Dugdale, R., Finkel, Z., Iudicone, D., Jahn, O., Guidi, L., Lasbleiz, M., Leblanc, K.,  
 1217 Levy, M., Pondaven, P.: Influence of diatom diversity on the ocean biological carbon  
 1218 pump, Nat. Geosci., 11, 27–37 (2018).

1219 Tréguer, P., Pondaven P.: Silica control of carbon dioxide, Nature, 406, 358–359, 2000.

1220 Tréguer, P.J. & De La Rocha, C.L.: The World Ocean silica cycle, Ann. Rev. Mar. Sci., 5, 477–  
 1221 501, 2013.

1222 Tréguer, P.J.: The Southern Ocean silica cycle, Comptes Rendus Geosci., 346, 279–286, 2014.

1223 Usbeck, U.: Modeling of marine biogeochemical cycles with an emphasis on vertical particle  
 1224 fluxes, PhD thesis, University Bremen, 1999.

1225 Von Damm, K.L., Bischoff, J.L. and Rosenbauer, R.J.: Quartz solubility in hydrothermal  
 1226 seawater: An experimental study and equation describing quartz solubility for up to 0.5  
 1227 M NaCl solutions, Am. J. Sci., 291, 977-1007, 1991.

1228 Wang W., Yang, S., Ran, X., Liu, X.-M., Bataille, C.P., & Su, N.: Response of the Changjiang  
 1229 (Yangtze River) water chemistry to the impoundment of Three Gorges Dam during  
 1230 2010–2011, *Chem. Geol.* 487, 1–11, 2018a.

1231 Wang, X., Baskaran, M., Su, K., Du, J.: The important role of submarine groundwater discharge  
 1232 (SGD) to derive nutrient fluxes into river dominated ocean margins – The East China  
 1233 Sea, *Mar. Chem.*, 204, 121–132, 2018b.

1234 Ward, B.A., Dutkiewicz, S., Jahn, O., & Follows, M.J.: A size-structured food-web model for  
 1235 the global ocean, *Limnol. Oceanogr.*, 57, 1877–1891, 2012.

1236 Westberry, T., Behrenfeld, M. J., Siegel, D. A., & Boss, E.: Carbon-based primary productivity  
 1237 modeling with vertically resolved photoacclimation. *Glob. Biogeochem. Cycles*, 22,  
 1238 GB2024, 2008.

1239 Wheat, C.G., & McManus, J.: The potential role of ridge-flank hydrothermal systems on  
 1240 oceanic germanium and silicon balances, *Geochim. Cosmochim. Acta*, 69, 2021–2029,  
 1241 2005.

1242 Wheat, C.G., & Mottl, M.J.: Composition of pore and spring waters from Baby Bare: global  
 1243 implications of geochemical fluxes from a ridge flank hydrothermal system, *Geochim.*  
 1244 *Cosmochim. Acta.*, 64, 629–642, 2000.

1245 Wischmeyer, A.G., De La Rocha, C.L., Maier-Reimer, E., & Wolf-Gladrow, D.A.: Control  
 1246 mechanisms for the oceanic distribution of Si isotopes, *Glob. Biogeochem. Cycles*, 17,  
 1247 1083, 2003.

1248 Wollast, R., Mackenzie, F.T.: Global biogeochemical cycles and climate, in: *Climate*  
 1249 *Geosciences: A challenge for science and society in the 21<sup>st</sup> century*, eds A. Berger,  
 1250 S.Schneider, & J.C. Duplessy (Dordrecht Springer), 453–473, 1989.

1251 Wu, B., Liu, S.M., & Ren, J.L. Dissolution kinetics of biogenic silica and tentative silicon  
 1252 balance in the Yellow Sea, *Limnol. Oceanogr.*, 62, 1512–152, 2017.

1253 Wu, B., Liu, S.M. Dissolution kinetics of biogenic silica and the recalculated silicon balance of  
 1254 the East China Sea. *Science of The Total Environment*, 2020.  
 1255 <https://doi.org/10.1016/j.scitotenv.2020.140552>

1256 Yang S. L., Xu, K.H., Milliman, J.D., Yang, H.F., & Wu, C.S.: Decline of Yangtze River water  
 1257 and sediment discharge: Impact from natural and anthropogenic changes, *Sci. Rep.*, 5,  
 1258 12581, 2015.

1259 Zhang, Z., Sun, X., Dai, M., Cao, Z., Fontorbe, G., Conley, D.J.: Impact of human disturbance  
 1260 on the biogeochemical silicon cycle in a coastal sea revealed by silicon isotopes, *Limnol.*  
 1261 *Oceanogr.*, 65, 515–528, 2019.

1262 Zhao, B., Yao, P., Bianchi, T., Xu, Y.: Early diagenesis and authigenic mineral formation in  
1263 mobile muds of the Changjiang Estuary and adjacent shelf, *J. Mar. Syst.*, 172, 64–74,  
1264 2017.  
1265

1266 **Table 1. Si inputs, outputs and biological fluxes at word ocean scale**

1267	<b>A-Estimates for Si inputs and outputs</b>		Reference	
1268	<b>Inputs</b> (in Tmol-Si yr <sup>-1</sup> )			
1269	F <sub>R(dSi + aSi)</sub> rivers	8.1 (±2.0)	Frings et al., (2016); Tréguer & De La Rocha (2013)	
1270	F <sub>A</sub> aeolian	0.5 (±0.5)	Tréguer & De La Rocha (2013)	
1271	F <sub>W</sub> dissolution lithogenic Si	1.9 (±0.7)	Tréguer & De La Rocha (2013)	
1272	F <sub>GW</sub> submar. groundwater	2.3 (±1.1)	Cho et al. (2018); Rahman et al. (2019); this review	
1273	F <sub>ISMW</sub> (sub)polar glaciers	0.3 (±0.3)	this review	
1274	F <sub>H</sub> hydrothermal	1.7 (±0.8)	this review	
1275	<b>Total inputs estimate</b>	<b>14.8 (±2.6)</b>		
1276				
1277	<b>Outputs</b> (in Tmol-Si yr <sup>-1</sup> )			
1278	F <sub>B(net deposit)</sub> burial	9.2 (±1.6)	this review, Hayes et al. (under review)	
1279	F <sub>SP</sub> sponges	1.7 (±1.6)	Maldonado et al. (2019)	
1280	F <sub>RW</sub> reverse weathering	4.7 (±2.3)	Rahman et al. (2016, 2017)	
1281	<b>Total outputs</b>	<b>15.6 (±2.4)</b>		
1282				
1283	<b>B-Comparative estimates of Si fluxes</b>			
1284		Ref. (1) & (2)	this review	Difference (%)
1285	<b>Net inputs</b> (Tmol-Si yr <sup>-1</sup> )	9.4 (±4.7)	14.8 (±2.6)	+57 %
1286	<b>Net outputs</b> (Tmol-Si yr <sup>-1</sup> )	11.4 (±7.6)	15.6 (±2.4)	+37 %
1287	<b>Gross bSi pelag. prod.</b> (Tmol-Si yr <sup>-1</sup> )	240 (±40)	255 (±52)	+06 %
1288	<b>D : P</b> (production: dissolution)	0.56	0.56	
1289				
1290	τ <sub>G</sub> residence time (kyears)	12.5 <sub>(3)</sub>	7.7	-38 %
1291	τ <sub>B</sub> residence time (kyears)	0.50 <sub>(3)</sub>	0.47	-6 %
1292	τ <sub>G</sub> : τ <sub>B</sub>	25 <sub>(3)</sub>	16	-34 %
1293	Refs. (1) Nelson et al. (1995) (2) Tréguer & De La Rocha (2013).			
1294	(3) recalculated from our updated dSi inventory value			
1295	See Supplement for detailed definition of flux term (in detailed legend of Fig. 1).			

1296  
1297  
1298  
1299  
1300



1301  
1302  
1303  
1304  
1305

**Table 2. Biological fluxes ( $F_{\text{Pgross}}$  in  $\text{Tmol-Si yr}^{-1}$ )**  
Global silica production as determined from numerical models and extrapolated from field measurements of silica production (uncertainties are standard errors)

Supprimé:

	World Ocean	Coast	Southern Ocean	Open Ocean
<b>Satellite Productivity models:</b>				
- Chlorophyll level	207 ( $\pm 23$ )	56 ( $\pm 18$ )	60 ( $\pm 12$ )	91 ( $\pm 2$ )
- Ocean Biogeochemical models	276 ( $\pm 22$ )		129 ( $\pm 19$ )	
<i>Average of models</i>	<b>242 (<math>\pm 49</math>)</b>			
<b>Silica production field studies:</b>				
- Ocean basin <sup>c</sup>	249			
- Domain <sup>c</sup>	285	138	67	80
<i>Average of field studies</i>	<b>267 (<math>\pm 18</math>)</b>			
<b>Global estimate</b>	<b>255 (<math>\pm 52</math>)</b>			

1306  
1307  
1308

**Table 3. Twenty-five years of evolution of the estimates for Si inputs, outputs, biological production, and residence times at world ocean scale**

References :	(1) Tréguer et al. (1995), (2) Tréguer & De La Rocha (2013), (3) this review, (4) Nelson et al. (1995)		
<b>A-Estimates for Si inputs and outputs fluxes</b>			
<i>References</i>	(1)	(2)	(3)
<b>Inputs (Tmol-Si yr<sup>-1</sup>)</b>			
F <sub>R(dSi + aSi)</sub> rivers	5.0 (±1.1)	7.3 (±2.0)	8.1 (±2.0)
F <sub>A</sub> aeolian	0.5 (±0.5)	0.5 (±0.5)	0.5 (±0.5)
F <sub>W</sub> dissolution lithogenic silica	0.4 (±0.3)	1.9 (±0.7)	1.9 (±0.7)
F <sub>GW</sub> submar. groundwater	-	0.6 (±0.6)	2.3 (±1.1)
F <sub>ISMW</sub> (sub)polar glaciers	-	-	0.3 (±0.3)
F <sub>H</sub> hydrothermal	0.2 (±0.1)	0.6 (±0.4)	1.7 (±0.8)
<b>Total inputs estimate</b>	<b>6.1 (±2.0)</b>	<b>9.4 (±4.7)</b>	<b>14.8 (±2.6)</b>
<b>Outputs (Tmol-Si yr<sup>-1</sup>)</b>			
F <sub>B(net deposit)</sub> burial	7.1 (±1.8)	6.3 (±3.6)	9.2 (±1.6)
F <sub>SP</sub> sponges	-	3.6 (±3.7)	1.7 (±1.6)
F <sub>RW</sub> reverse weathering	-	1.5 (±0.5)	4.7 (±2.3)
<b>Total outputs estimate</b>	<b>7.1 (±1.8)</b>	<b>11.4 (±7.6)</b>	<b>15.6 (±2.4)</b>
<b>B-Estimates for Gross production of biogenic silica (Tmol-Si yr<sup>-1</sup>)</b>			
<i>References</i>	(4)	(3)	
Gross production of biogenic silica	240 (±40)	255 (±52)	
<b>C-Residence time of Si (kyears)</b>			
<i>References</i>	(1)	(2)	(3)
τ <sub>G</sub> residence time (geological)	18.3 <sup>(5)</sup>	12.5 <sup>(5)</sup>	7.7
τ <sub>B</sub> residence time (biological)	0.50 <sup>(5)</sup>	0.50 <sup>(5)</sup>	0.47
τ <sub>G</sub> : τ <sub>B</sub>	37 <sup>(5)</sup>	25 <sup>(5)</sup>	16
<sup>(5)</sup> recalculated from our updated dSi inventory value			

1342 **Figure 1:** Schematic view of the Si cycle in the modern world ocean (input, output, and  
1343 biological Si fluxes), and possible balance (total Si inputs = total Si outputs = 15.6 Tmol-Si yr<sup>-1</sup>)  
1344 in reasonable agreement with the individual range of each flux (F), see Tables 1 and 2. The  
1345 white arrows represent fluxes of net sources of silicic acid (dSi) and/or of dissolvable  
1346 amorphous silica (aSi) and of dSi recycled fluxes; Orange arrows correspond to sink fluxes of  
1347 Si (either as biogenic silica and or as authigenic silica); Green arrows correspond to biological  
1348 (pelagic) fluxes. All fluxes are in teramoles of silicon per year (Tmol-Si yr<sup>-1</sup>). Details in  
1349 Supplement section 1.

1350 **Figure 2.** Schematic view of the low temperature processes that control the dissolution of  
1351 (either amorphous or crystallized) siliceous minerals in seawater in and to the coastal zone and  
1352 in the deep ocean, feeding  $F_{GW}$  and  $F_w$ . These processes correspond to both low and medium  
1353 energy flux dissipated per volume of a given siliceous particle in the coastal zone, in the  
1354 continental margins, and in the abysses, and to high-energy flux dissipated in the surf zone.  
1355 Details in Supplement section 1.

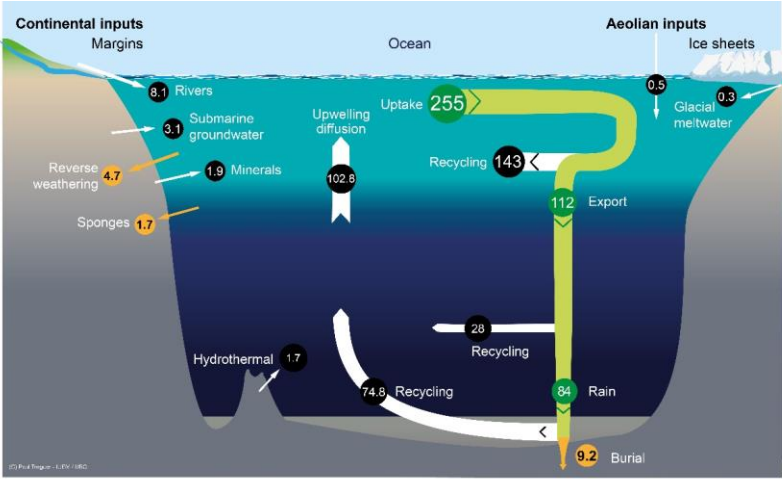
1356 **Figure 3.** Biogenic silica production measurements in the world ocean. Distribution of  
1357 stations in the Longhurst biogeochemical provinces (Longhurst, 2007; Longhurst et al., 1995).  
1358 All data are shown in Supplement, section 4 (Annex 1).

1359 **Figure 4.** Schematic view of the Si cycle in the coastal and continental margin zone (CCMZ),  
1360 linked to the rest of the world ocean (« open ocean » zone, including upwelling and polar  
1361 zones). In this steady-state scenario, consistent with Fig. 1, total inputs = total outputs = 15.6  
1362 Tmol-Si yr<sup>-1</sup>. This figure illustrates the links between biological, burial and reverse weathering  
1363 fluxes. It also shows that the “open ocean” bSi (pelagic) production ( $F_{P(gross)} = 222$  Tmol-Si yr<sup>-1</sup>)  
1364 is mostly fueled by dSi inputs from below (92.5 Tmol-Si yr<sup>-1</sup>), the CCMZ only providing 4.7  
1365 Tmol-Si yr<sup>-1</sup> to the “open ocean”.

1366

1367

1368    Figure 1(provisional)

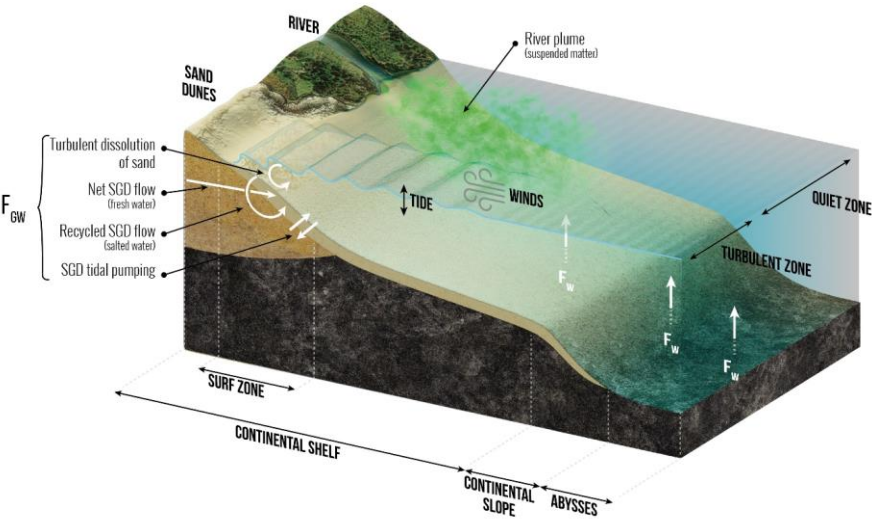


1369

1370

1371

1372    Figure 2



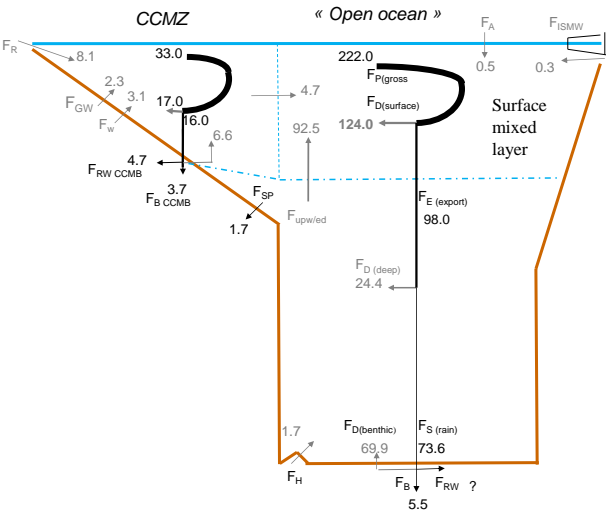
1373

1374

1376  
1377



1378    Figure 4



1379

1380